2 TOTAL SYSTEM CODE

2.1 DESCRIPTION OF IPA PHASE 2 TOTAL SYSTEM CODE

2.1.1 Performance Assessment Approach

The U.S. Nuclear Regulatory Commission (NRC) has the statutory responsibility for evaluating the license application for construction, operation, and closure of a high-level waste (HLW) geologic repository. Issuance of a license for a HLW repository will require a finding that the repository not constitute an unreasonable risk to public health and safety [10 CFR 60.31(a)]. In arriving at a licensing decision, the NRC will evaluate the repository against applicable regulations promulgated by the NRC (10 CFR Part 60) and the U.S. Environmental Protection Agency (EPA) (40 CFR Part 191). In this study, principal focus is on modeling the performance of the total system and assessing compliance with the EPA Standard.

Postclosure performance assessment (PA), as a primary evaluation process, will provide the scientific basis for judging the acceptability of the geologic repository. The EPA regulation [40 CFR 191.12(q)] defines and describes PA for the overall system as:

> *"... an analysis that (1) identifies processes and events that might affect the disposal system; (2) examines the effects of these processes and events on the performance of the disposal system; and (3) estimates the cumulative releases of radionuclides, considering the associated uncertainties, caused by all significant processes and events. These estimates shall be incorporated into an overall probability distribution of cumulative release to the extent practicable."*

A broader definition of PA, that applies to both the overall system and its components (i.e., subsystems), can be drawn from the concepts expressed in the NRC regulation (10 CFR Part 60), wherein it is reflected that PA is the process of quantitatively evaluating the natural and engineered repository components and the overall repository system behavior, relative to the performance objectives of 10 CFR Part 60.

Implicit in these two definitions is the concept that PA will use mathematical models to predict the future behavior of the repository. Development of these models is a challenging undertaking because it requires the integration of the scientific principles and knowledge bases from many diverse disciplines. Added to the modeling difficulty is the need to account for uncertainty in data and future states as well as those in the conceptual models and physicochemical theories.

To make the mathematical modeling realistic as well as computationally feasible, the NRC approach to PA involves the use of a hierarchy of models (see Figure 2-1). In this approach, the total-system model is at the top of the hierarchy and it describes diverse phenomena (e.g., fluid flow, heat transport, geochemistry, corrosion, etc.) to relate the performance of the overall system to its components. The total-system model is formulated in a probabilistic framework to propagate the uncertainty in model parameters and future states. Mid-level in the hierarchy are the subsystem models that are tailored for computation of individual performance objectives for the natural and engineered components of the repository. These mathematical models are more detailed (e.g., coupled descriptions

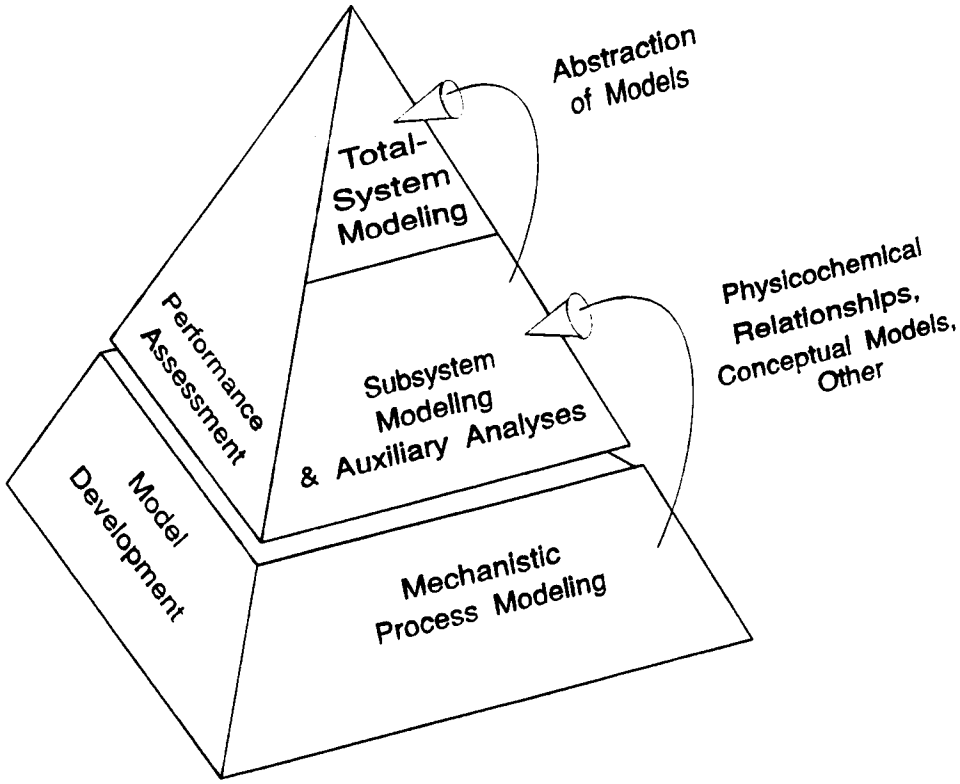

Figure 2-1. PA model hierarchy (After Barnard et al., 1992)

of phenomena, greater spatial and temporal discretization) but are restricted to selected phenomena. They are often used in auxiliary analyses to support the total-system model. The mathematical models at the bottom of the hierarchy describe unique phenomena and are used to generate input for models in the upper and mid-levels of the hierarchy.

The basic components of the current NRC methodology (Codell et al., 1992) for conducting total-system performance assessments for the proposed geologic repository consist of six general steps: (i) system description; (ii) scenario analysis; (iii) consequence analysis; (iv) performance measure calculation; (v) sensitivity and uncertainty analysis; and (vi) documentation.

2.1.2 Description of Total-System Code

2.1.2.1 Introduction

The objective of the Total Performance Assessment (TPA) code is to provide computational algorithms for estimating the complementary cumulative distribution function (CCDF) for releases to the accessible environment. Such computations will take into account the interactions among subsystems, components, future states, and processes. When fully developed, the TPA system will permit estimates of system performance as a function of the specific characteristics of the proposed repository site.

The diverse nature of the physicochemical processes being simulated requires that theories from many disciplines be integrated into an overall system mode. Consequently, it is desirable to design the

TPA as a set of Consequence Modules (CM) which are largely independent computational units with their execution controlled by an executive module. The executive module acts as the controller and executes the CMs in the desired sequence and ensures that appropriate values of the common parameters are passed to CMs. Automated features included in the system facilitate the unattended running of a set of multiple scenarios with associated output.

A complete description of the TPA code is available in the Center for Nuclear Waste Regulatory Analyses (CNWRA) document CNWRA 91-009 (Sagar and Janetzke, 1991). The requirements for the TPA were developed early in the design process. The TPA code was developed using software utilities designed to increase the productivity of the developers and the quality of the final product. One of these was the "preFOR" FORTRAN preprocessor utility, which is described in the document CNWRA 91-003 (Janetzke and Sagar, 1991a).

2.1.2.2 Code Organization

Organizationally, the TPA system code consists of four basic parts: (i) the executive (or manager); (ii) algorithm(s) to sample from statistical distributions; (iii) algorithm(s) to model future states or scenarios, and (iv) algorithms to model transport processes. Consequences are quantified in terms of cumulative releases and dose-to-man. In addition, algorithms to compute sensitivities and perform uncertainty analyses are executed separately as an auxiliary process. The parts listed under (ii) and (iii) are called subprocesses in the following description. The executive of the TPA directs data flow between different parts and controls their execution. It is this executive part that is discussed in this section. The executive module of the TPA system code currently consists of about 21,000 lines of FORTRAN, while the complete system code is about 85,000 lines. Figure 2-2 shows schematically the data flow and execution dependencies of the subprocesses of the TPA system code.

The CM programs, which are used as subprocesses, are designed such that they may also be executed by themselves (stand-alone) without the aid of the TPA system. The standard documentation prepared for these programs will also apply to their use in the TPA system, with minor modifications to input and output procedures which are explained in the TPA Code Description document. The TPA system uses a dedicated subroutine to handle the setup and initiation of each subprocess. An additional subroutine is required to read any results which may be provided to the executive by a particular subprocess. The subprocess is created as the result of a CALL to a utility routine, which is specific to the operating system. This CALL is the mechanism which starts the subprocess. Control is returned to the executive module at the end of the execution of the subprocess.

The subprocess for obtaining samples from specified statistical distributions is based on the Latin Hypercube Sampling (LHS) method (Inman and Shortencarier, 1984). The LHS program was obtained from Sandia National Laboratory (SNL). Other programs used as subprocesses include algorithms for computing flow fields, estimation of doses, and calculation of consequences of scenarios such as human intrusion. Modules to calculate sensitivities of the final results (e.g., CCDF) to selected parameters are implemented as external auxiliary processes.

2.1.2.3 Data Handling and Control

The TPA Input/Output (I/O) files can generally be divided into four different types: (i) input; (ii) temporary (used for the duration of the current scenario); (iii) reusable (used for more than one scenario); and (iv) output. The input files include the TPA input file, LHS standard input file, and

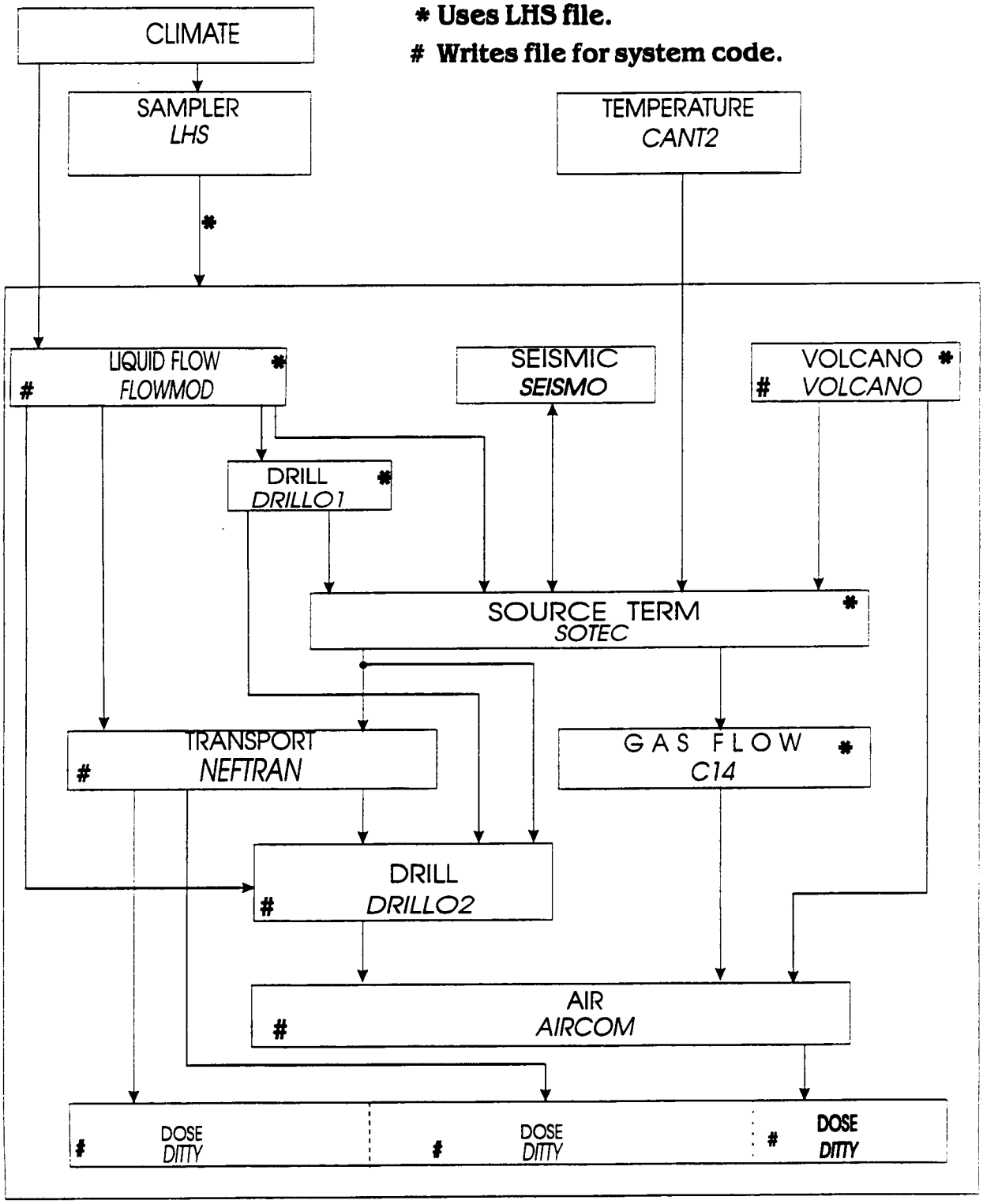

Figure 2-2. Organization of the TPA computer code

standard input files for each of the CMs. The TPA input file is prepared in a free format style. That is, the input values are associated with keywords rather than with fixed column positions in the input file. This was implemented using a set of standard FORTRAN routines described in document CNWRA 91-005 (Janetzke and Sagar, 1991b).

The temporary files include the files generated by the TPA system for the purpose of transmitting control parameters to an external module. These typically contain global parameters (parameters that are common to more than one module) which can override the parameters read from the module's standard input file. The temporary files receive their names from the TPA Executive and are overwritten for each new vector processed. In general, only the programmer (and not the end user) needs to accommodate the temporary files.

The reusable files are those on which intermediate results from various CMs are written. The data in these files may be processed later by other modules. For example, the releases of radionuclides calculated by a CM (e.g., human intrusion) will be written on a reusable file. These files are saved and can later be used to analyze intermediate results.

The output files include the output file of the TPA, standard output files of each one of the CMs, error log files, and specially formatted files for external utilities such as the TECPLOT graphics utility (TECPLOT, 1984).

Names of all files except the temporary files can be read as part of the input. The format-free input process of the TPA Executive is explained in the TPA Documentation. This format-free input is keyword based.

2.1.2.4 Sampled Data

Many of the CMs require some of their input variables to be sampled with a certain distribution over a range with known end points. This feature is adapted in a common manner for all of the modules involved. The LHS program is used to generate the sampled data for all of the variables, and for all vectors of a given scenario. A standard LHS input file is created with distribution specifications for all of the variables. LHS then produces a single output file containing a data set for each vector. When each module begins execution it reads this file sequentially until it finds the correct vector and then reads the entire variable set for that vector. The module must then select its variables from this set as specified in a "map" file which identifies the location of each variable.

When the modules are executed in a stand-alone mode sampled variables are not used, and all of the necessary control input is provided via the standard input file. In the TPA system, however, the sampled data must override any values provided in the standard input file. This is done by assuring that the sampled data is read after the standard input file is read, and before any quantities are derived from them.

One of the primary requirements of the simulation process is that parameters that are common to many subprocesses be consistent among these subprocesses. Since the design of the TPA is such that all the subprocesses can run independently, this consistency is maintained through the temporary global data files which transmit data from the executive to the CMs. These data files contain parameters in a fixed order and the corresponding CM must follow this order when extracting the parameters from the file. This process is completely automated and does not require manipulation by the user.

2.2 IMPROVEMENTS AND CHANGES SINCE PHASE 1

The Phase 1 system code was developed to the point where LHS and the NEtwork Flow and TRANsport code (NEFTRAN) (Longsine, et al., 1987) can run in internal or external mode, with sensitivity analysis and CCDF generation performed on an auxiliary basis. The external mode was the only mode demonstrated for the system code. This mode required the analyst to prepare all of the necessary files for LHS, NEFTRAN, and CCDF presentations. Five hundred vectors were run for the base case and the drilling only scenario. However, only 98 vectors were run for the pluvial cases. The repository site was assigned 4 zones, and the calculations were done for 29 nuclides in each zone.

By contrast, the Phase 2 system code was developed to run 16 scenarios with all combinations of the 4 disruptive events: (i) pluvial; (ii) seismic; (iii) drilling; and (iv) volcanic. The execution of the scenarios is performed under the control of the system executive with consistent data provided automatically to all of the CMs. The system executive is responsible for the invocation of the modules and the reading of the release values after each module is run. A single array is used in the executive to store the release values organized by nuclide, pathway, zone, module, vector, and scenario. After the values have been normalized the CCDF is generated from this array.

While both internal and external modes are available for the TPA executive, the internal mode is preferred. This mode assures that all of the modules receive the same input data for common control and data variables. The individual modules obtain much of their control and data information from the system executive, thereby the executive exercises a degree of precision when invoking the module to execute a particular scenario or vector. The communication mechanism used for this is formatted ASCII files. These files are called global data files, since much of the content is common to the consequence modules.

The LHS program was implemented in a way that does not increase in complexity when additional CMs are added to the system. All the sampled variables from all of the modules are generated during a single run of the LHS code, and then each module can select its sampled variables from the file using identical techniques. A mapping file serves to aid the module in extracting the correct variables from the LHS output file since the LHS program does not organize its output with keys for each variable. The map file contains the exact location of each sampled variable for a given module.

In Phase 2 the repository was divided into 7 zones and the normalized release values were stored separately for each zone as well as each of the 29 nuclides. In addition, several new CMs were added to the system, namely groundwater travel time, seismic, volcanic, C14 gas flow, and dose calculation modules.

The TPA executive can produce a CCDF plot in TECPLOT (TECPLOT, 1984) format for each scenario, as well as a total CCDF for all of the scenarios, from the single internal array which stores the normalized release values from all of the CMs.

2.3 AUXILIARY ANALYSES

In general, auxiliary analyses are conducted to examine specific processes and factors that may be important to total-system performance. These processes and factors are evaluated using more detailed

models to: (i) provide greater insight to cause-and-effect relationships; (ii) evaluate conservatism of model assumptions; (iii) evaluate alternate modeling approaches; and/or (iv) interpret field and laboratory data.

For the Iterative Performance Assessment (IPA) Phase 2 analysis, eight distinct auxiliary analyses were performed. These analyses included:

- Evaluation of the SNL flow and transport codes
- Evaluation of flow model assumptions
- Analysis of regional groundwater flow
- Two-dimensional analysis of unsaturated flow
- Analysis of ^{14}C transport
- Evaluation of K_d approximation
- Effects of layering and dipping
- Review of USGS regional flow modeling

Detailed descriptions of these auxiliary analyses are given in section 4.5.

2.4 REFERENCES

TECPLOT. 1984. *TECPLOT User's Guide, Version 3.5.* Bellvue, WA: Amtec Engineering, Inc.

Codell, R.B., N.A. Eisenberg, D.J. Fehringer, W.H. Ford, T. Margulies, T.J. McCartin, J.R. Park, and J.D. Randall. 1992. *Initial Demonstration of the NRC's Capability to Conduct a performance Assessment for a High-Level Waste Repository.* NUREG/CR-1327. Washington, DC: U.S. Nuclear Regulatory Commission.

Inman, R.L., and M.J. Shortencarier. 1984. *A FORTRAN 77 Program and User's Guide for the Generation of Latin Hypercube and Random Samples for Use in Computer Models.* NUREG/CR-3624, SAND 83-2365. Albuquerque, NM: Sandia National Laboratories.

Janetzke, R., and B. Sagar. 1991a. *preFOR: A Pre-Processor for FORTRAN Files, User's Manual.* CNWRA 91-003. San Antonio, TX: Center for Nuclear Waste Regulatory Analyses.

Janetzke, R., and B. Sagar. 1991b. *RDFREE: A FORTRAN Utility for Format Free Input, User's Guide.* CNWRA 91-005. San Antonio, TX: Center for Nuclear Waste Regulatory Analyses.

Longsine, D.E., E.J. Bonano, and C.P. Harlan. 1987. *User's Manual for the NEFTRAN Computer Code*. NUREG/CR-4766. Washington, DC: U.S. Nuclear Regulatory Commission.

Sagar, B., and R. Janetzke. 1991. *Total System Performance Assessment Computer Code: Description of Executive Module*. CNWRA 91-009. San Antonio, TX: Center for Nuclear Waste Regulatory Analyses.

4 FLOW AND TRANSPORT MODULE

4.5.3 Regional Flow Analysis

4.5.3.1 Introduction

Assessing the overall long-term performance of the proposed high-level nuclear waste (HLW) geologic repository at Yucca Mountain requires predictions of the impact of postulated disruptive events occurring over the 10,000-year isolation period of regulatory interest. Such predictions will usually be made through the use of computer modeling techniques. One area which has received much recent attention is the likelihood in the future for significant rises in the water table beneath Yucca Mountain due to possible events such as seismic activity, increased precipitation over the region, volcanic intrusions, or changes to existing hydrogeologic barriers. Such events could lead to, for instance, a significant change in the rates of water flow through the unsaturated zone beneath the repository horizon due to alterations in the unsaturated zone.

As one of the auxiliary analyses in the Iterative Performance Assessment (IPA) Phase 2, it was decided to simulate the flow field in the saturated unconfined region that contains Yucca Mountain. The specific objective of this analysis is to study the fluctuations in the water table in response to postulated changes in recharge rates and other modifications in geohydrologic structures. The simulations were conducted both on a regional scale as well as a smaller scale, i.e., the scale of Yucca Mountain. The regional scale analysis provided the boundary conditions for the simulations of the saturated zone in the subregional model. A full discussion of this analysis and results is given in a recent report by Ahola and Sagar (1992).

Because of the limited objective of the analysis presented in this report, no attempt was made to estimate the probability of occurrence of such events mentioned above. Only data that were readily available from other published reports were used. Also, some parameter values were taken from other published reports (e.g., Rice, 1984; Waddell, 1982; and Czarnecki, 1985) without verifying their accuracy. Consequently, the analysis results should be considered as preliminary and likely to change when more detailed field data are used in the simulations. In addition, evapotranspiration and modifications in surface runoff were not considered.

The simulation results pertain to a two-dimensional (2D) regional (about 250 $\times$ 250 km) and subregional (50 $\times$ 50 km) area, and saturated groundwater flow analysis beneath Yucca Mountain and the surrounding area. For this application, PORFLOW (Runchal and Sagar, 1989; Sagar and Runchal, 1990), an integrated finite difference code, was modified (Version 1.11) to incorporate the free surface (water table) in a groundwater flow model. The model was set up in the x-y (horizontal) plane, and allowed for specification of recharge and discharge areas. An approximate model of the regional groundwater flow system around Yucca Mountain was first developed for the PORFLOW code. Once this was completed, various conditions were postulated, such as increasing the recharge to simulate future adverse climatic changes that might take place in the geohydrologic basin containing Yucca Mountain.

4.5.3.2 Relevant Literature

A brief summary of relevant literature pertinent to saturated zone modeling that was reviewed for this study follows; comprehensive literature review of all hydrologic studies in the Yucca Mountain area was not conducted. A more detailed discussion of previous studies of the saturated zone hydrology is given by Ahola and Sagar (1992), and can also be found in the Site Characterization Plan (SCP) [Department of Energy (DOE), 1988]. The purpose of this review was mainly to determine what other modeling studies were conducted to simulate the regional saturated hydrology, and to utilize the results and data (i.e., hydraulic conductivities and boundary conditions) from such studies for the PORFLOW analysis. These previous studies were more comprehensive in that their models were calibrated on measured heads. For this study, no model calibration was done; rather, parameter values from previous studies were adopted.

Waddell (1982) conducted flow modeling on a regional basis for the Nevada Test Site and vicinity. The main goals of his investigation were: (i) to estimate fluxes for use in predictions of transport of radionuclides; and (ii) to study the effects of uncertainty in model parameters on these estimates. Waddell used a horizontal 2D finite-element model consisting of 685 nodes. The model encompassed an area approximately 175 × 175 km, the boundaries of which were taken mainly along topographic highs to the north and east, and topographic lows to the southwest. For model calibration, a numerical parameter-estimation technique was used in which parameters such as transmissivities, groundwater sources, and sinks were derived throughout the modeled area such that the weighted sum of the squared residuals (observed head minus simulated head) was minimized. An iteration scheme was used to minimize the weighted sum of squared residuals by successive approximation to model parameters. It was generally found that absolute values of residuals were less than 30 m.

Czarnecki and Waddell (1984) developed a subregional horizontal finite-element model of the groundwater flow system in the vicinity of Yucca Mountain also using parameter estimation techniques. This model was formulated as a portion of the regional model conducted by Waddell (1982). Some of the boundaries for this subregional model were taken along groundwater barriers from the larger regional model. The remaining boundaries had either specified pressure heads or fluxes, which were calculated from the regional model. The purpose of this subregional model study was to gain a better understanding of the groundwater flow system beneath the Yucca Mountain area. Czarnecki (1985) used this same 2D finite-element subregional model to assess the potential effects of changes in future climatic conditions on the groundwater system in the vicinity of Yucca Mountain. He found that the simulated position of the water table rose as much as 130 m near the primary repository area at Yucca Mountain for a simulation involving a 100 percent increase in precipitation compared to current conditions. The average increase in recharge for the case of this 100 percent increase in annual precipitation was set at 15 times the modern-day recharge rate in all areas of his model. The primary factor in this water table rise was due to the increase in recharge applied to Forty Mile Wash to the east of Yucca Mountain by a factor of 15 times the baseline rate of 0.41 mm/yr. For a factor of 10 increase in flux into the model, Czarnecki shows an increase in hydraulic head near Yucca Mountain of approximately 100 m. Flooding on the primary repository area would require a water table rise of at least 300 m.

Rice (1984) also developed a 2D regional hydrologic model for the saturated flow system surrounding Yucca Mountain. A finite-difference grid consisting of 5,600 nodes in the x-y plane was used for the simulations. The flow system was modeled under confined conditions, and only horizontal flow was allowed. Model calibration was accomplished by adjusting the transmissivities within reasonable limits in order to minimize the difference between the hydraulic heads simulated by the model

and hydraulic heads measured at well locations. Results of simulated heads compared closely with U.S. Geological Survey (USGS)-interpreted head distribution based on well observations.

4.5.3.3 Description of Analyses

Conceptual Models and Data: The conceptual models for this analyses consisted of both a regional model (approximately 250 × 250 km), and a subregional model (50 × 50 km), set up in the x-y (horizontal) plane as shown in Figure 4-1. Provision was made to allow for specification of recharge and discharge areas in the model. The primary recharge was assumed to occur on outcrops at higher elevations, as shown in Figure 4-1. Current estimates of recharge in these areas range from approximately 7 to 200 mm/yr depending primarily on the land surface elevation as given by Rice (1984). Discharge areas included Alkali Flats and the Furnace Creek Ranch, which were modeled as fixed head boundaries. Mathematical boundary conditions for the regional model consisted of both fixed pressures and no-flow boundaries; these boundary conditions were chosen to be consistent with the physical boundaries (Figure 4-1). The regional and subregional models consisted of 13,161 and 18,225 finite difference computational cells, respectively. Each grid cell in the regional model was 2.5 km on a side, encompassing an area of 6.25 km^2. The grid cells for the subregional model ranged from 100 m on a side near the center to 2.5 km on a side near the outer edges. The boundary conditions for this model consisted only of fixed pressures which were obtained from the simulation results of the larger regional model. The hydrological data for the simulations were obtained from the review of previously published studies (Rice, 1984; Waddell, 1982; Waddell et al., 1984; Czarnecki and Waddell, 1984; and Czarnecki, 1985).

The entire modeled region was divided into zones having one of eight possible values for the hydraulic conductivity as shown in Figure 4-2 and listed in Table 4-1. These hydraulic conductivities varied over several orders of magnitude, and were estimated from transmissivity data published by Rice

Table 4-1. Hydraulic conductivities for the model

Zone Number	Hydraulic Conductivity (m/sec)
1	5.80E-08
2	6.34E-07
3	3.49E-06
4	8.69E-06
5	3.47E-05
6	1.00E-04
7	6.00E-04
8	3.50E-03

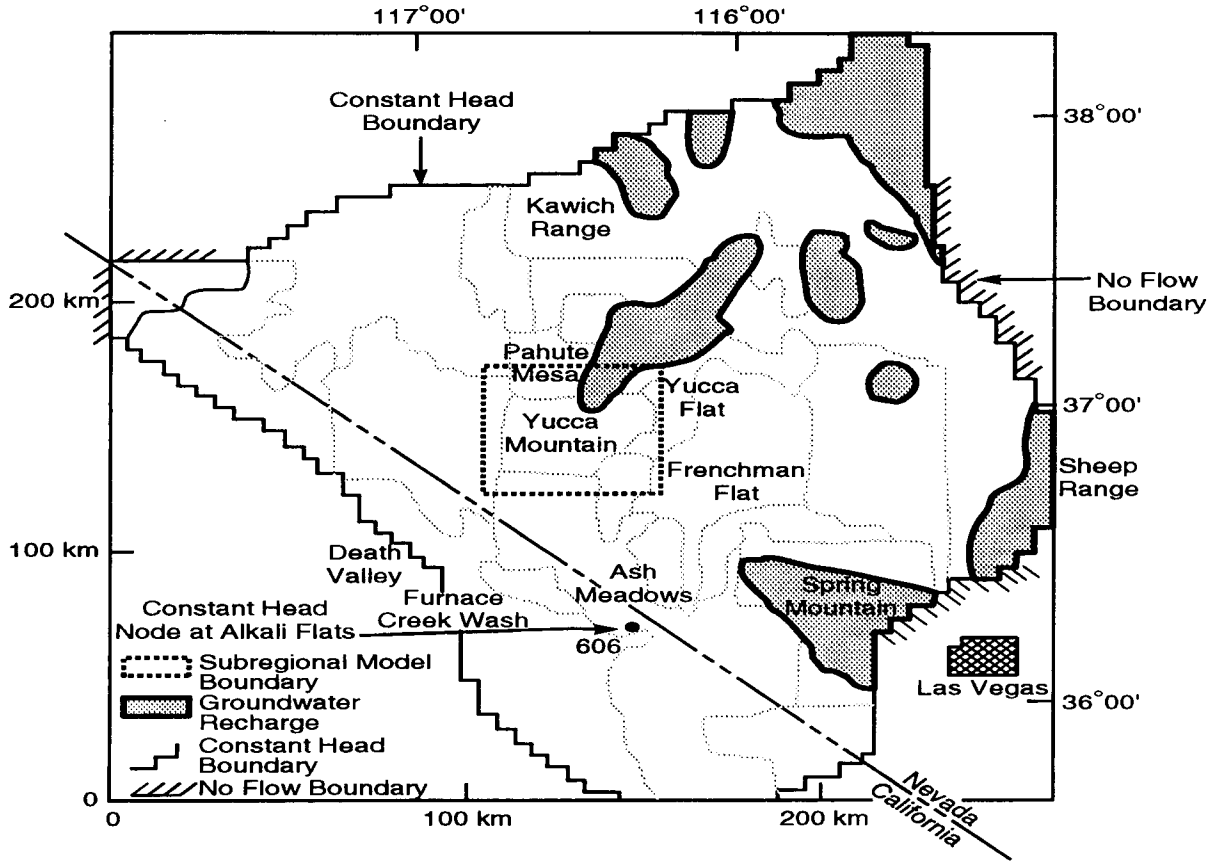

Figure 4-1. Regional and subregional models for PORFLOW depicting location of recharge and constant head discharge areas (modified from Rice, 1984)

(1984). The model contains a low permeability zone north and northeast of Yucca Mountain for simulating the present-day high hydraulic gradient at that location. The actual cause of the steep gradient is not yet fully known.

To conduct the study, PORFLOW was modified (Version 1.11) to incorporate the free surface (water table) in a groundwater flow model. The free-surface boundary condition and approximations (e.g., Dupuit) used in the modifications to PORFLOW are described in Bear (1972). Detailed discussion of the specific modifications to PORFLOW is given by Ahola and Sagar (1992).

4.5.3.4 Analyses Results

Regional Model Results: For the regional analysis, a steady-state solution to the flow system was first obtained to represent the present-day conditions under normal precipitation and groundwater recharge. Figure 4-3 shows a portion of the simulated regional water table in the area of interest under assumed modern day recharge. Yucca Mountain is indicated by the small rectangular box in this figure and represents approximately two grid nodes in the regional model. Thus, on the Yucca Mountain scale, the regional model is quite coarse. Based on the simulation, one can see the steep hydraulic gradient to the north and northeast of Yucca Mountain, which is comparable to results obtained in previous studies. It should be noted, however, that no calibration of this model was conducted for this study. The results

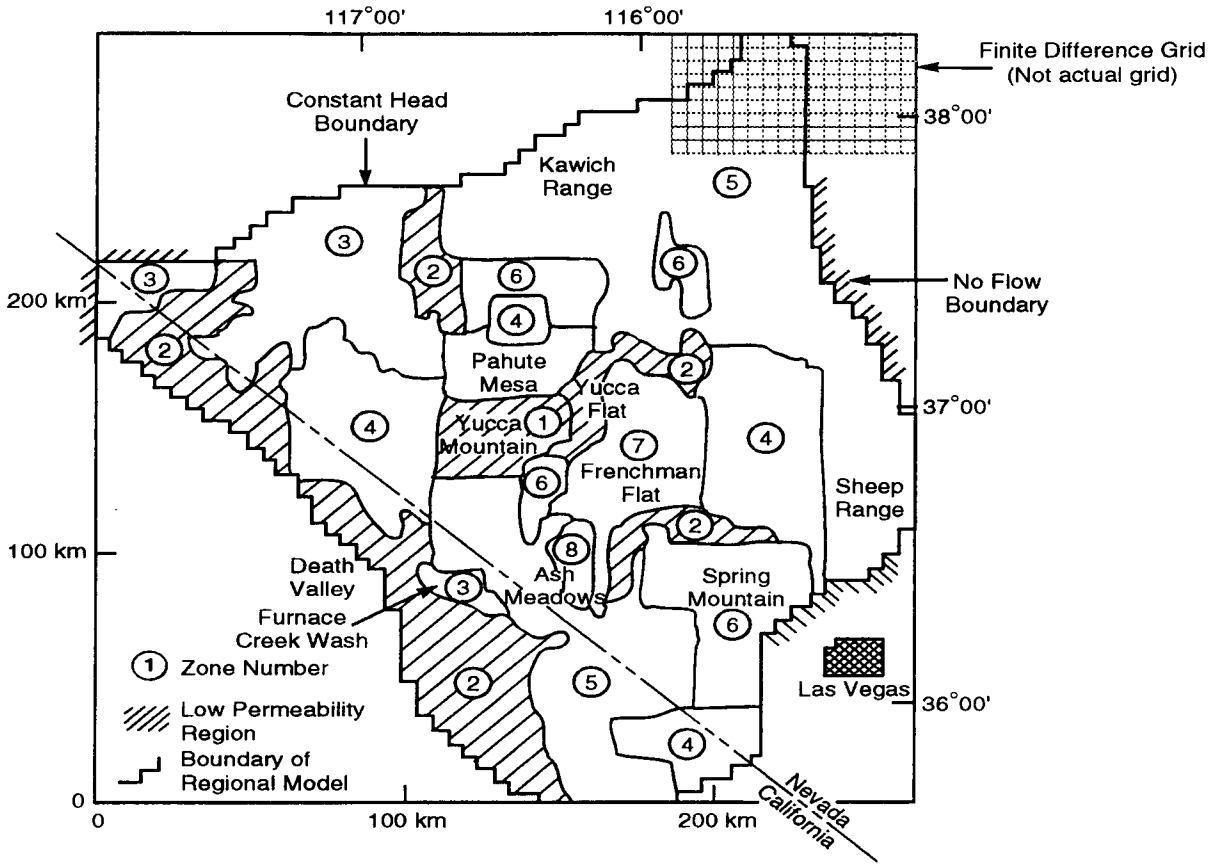

Figure 4-2. Regional model for PORFLOW depicting boundary conditions and various hydraulic conductivity zones (modified from Rice, 1984)

are based on the use of data published from previously calibrated models. Since the results appeared consistent with previous studies and our objective was to focus more on relative changes in the water table rather than on the absolute water table elevation itself, they were deemed acceptable for use as a base case or initial state for analyzing the effects of various postulated disruptive conditions.

One possible condition which could occur over the 10,000-year isolation period for a repository at Yucca Mountain would be increased precipitation and groundwater recharge throughout the region. Such groundwater recharge is thought to be greatest in the higher elevations where there is more precipitation and outcropping of the basement rock. Figure 4-4 shows a relationship between increased recharge and water table rise at nodal points in the vicinity of Yucca Mountain and 5 km to the east at Forty Mile Wash. The numbers representing increase in recharge as shown on the x-axis are multipliers of the baseline (present-day) flux. The recharge is applied over those shaded regions indicated in Figure 4-1. The results show a more or less linear relationship between the two parameters. In general, from the transient analysis, a larger increase in recharge resulted in a longer period of time in which the groundwater flow field reached steady-state. For instance, the simulated water table configuration took approximately 400 years to equilibrate when the recharge was increased 10 times and 700 years to equilibrate when the recharge was increased 20 times. Czarnecki (1985) states that a 100 percent increase in annual precipitation over the region would correspond to an increase in groundwater recharge of approximately 15 times the present-day recharge rate. From Figure 4-4, this would correspond to a water

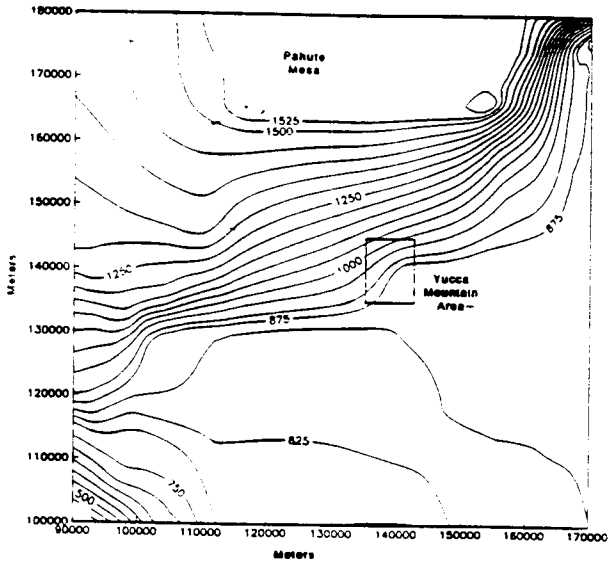

Figure 4-3. Simulated hydraulic head distribution in the vicinity of Yucca Mountain under assumed present-day conditions

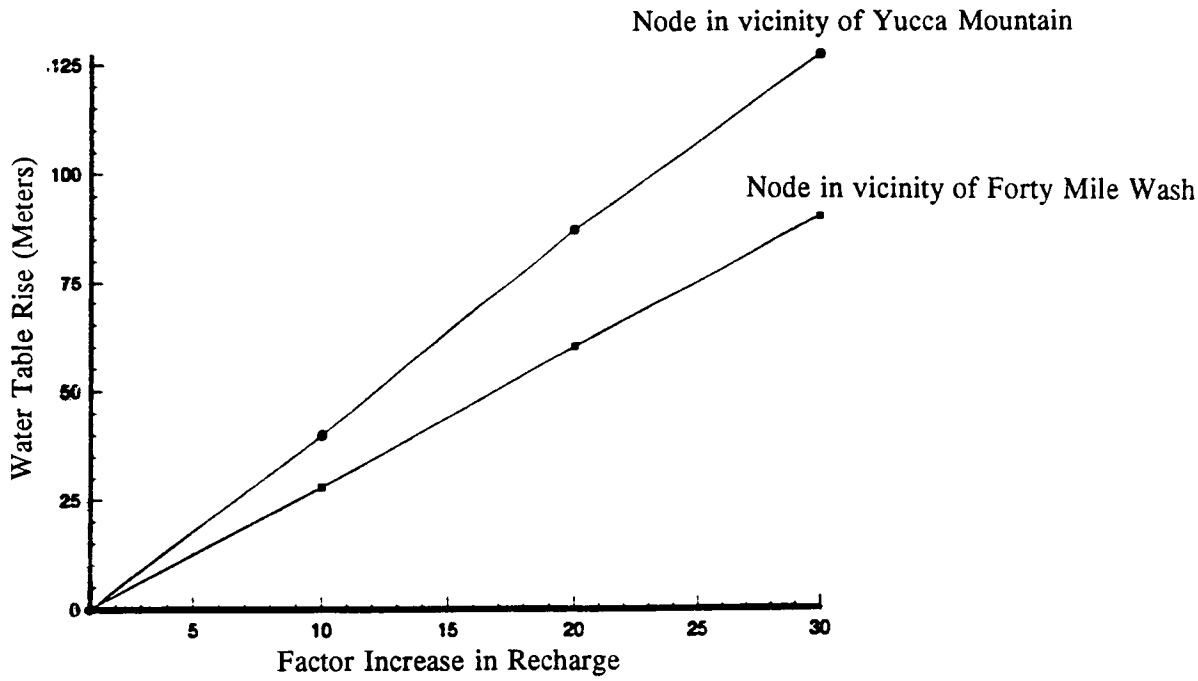

Figure 4-4. Water table rise at Yucca Mountain and Forty Mile Wash as a function of recharge rate

table rise at Yucca Mountain of approximately 65 m. Czarnecki (1985) found that, in addition, increasing the recharge into Forty Mile Wash above a small annual baseline recharge had a significant effect on the water table rise near Yucca Mountain, primarily due to its close proximity. It is conceivable that increased precipitation in the higher elevations would cause greater runoff into Forty Mile Wash, for example, and consequently greater recharge. The results shown in Figure 4-4, however, assume no recharge into Forty Mile Wash.

As another potentially disruptive condition, it was postulated that future tectonic activity throughout the Basin and Range region could result in slip or opening of fractures through the areas north and northeast of Yucca Mountain where large hydraulic gradients exist, and increase the flow towards Yucca Mountain. While the exact cause is not well understood, it is thought that these large gradients may be due to the fact that a low permeability geologic unit has been jutted against a high permeability unit, or perhaps that large lateral tectonic stresses within this region have closed existing north-south trending fractures. This condition was simulated in the regional model by increasing, to various degrees, the permeabilities through the previous low permeability regions just to the north (zone 1) and northeast (zone 2) of Yucca Mountain, as shown in Figure 4-2. The relationship between the increase in permeability through these two zones and the subsequent rise in the water table at nodal points near Yucca Mountain and Forty Mile Wash is shown in Figure 4-5. The numbers along the x-axis represent multipliers of the assumed present-day permeabilities in the two zones directly north and northeast of the Yucca Mountain repository site. Figure 4-5 shows that a fairly substantial rise in the water table can be expected for even a factor of 10 increase in the permeability of these two zones. If the permeability of these two zones is increased to a value representative of the hydraulic conductivity of zone number 7 (Table 4-1), which is approximately 1,000 times greater, the modeling results show a water table rise in the area of Forty Mile Wash over 200 m. In this case, the steep gradient north and northeast of Yucca Mountain no longer exists.

Subregional Model Results: To study the impact of volcanic dike intrusions occurring directly beneath Yucca Mountain in more detail, an analysis was conducted using a smaller scale subregional model. These dikes were assumed to be approximately 4 km in length and extend vertically through the saturated zone. For these simulations, the regional model was too coarse. The location of the subregional model is depicted by the dashed rectangular region in Figure 4-1. The finite-difference grid encompassed an area of 50 x 50 km. The grid cells were 100 m on a side near the center of the mesh where the volcanic dikes were assumed to be located. At the outer boundaries of the model, the largest grid cells were 2.5 km on a side, which corresponded to the size of the grid cells for the regional model. The boundary conditions along all four sides of this model consisted of fixed pressures obtained from corresponding nodes in the regional model. Linear interpolation was done to assign values of pressure to those additional nodes along the boundary of the subregional model as a result of refining the mesh. These fixed boundary pressures corresponded to the baseline (or current) water table configuration from the regional model.

No attempt was made to take into account the effect the temperature of the intruding dike might have on the saturated zone. The narrow dikes essentially acted as dams within the flow field, and were assumed to extend through the water table and well above any potential water table rise. They were created by specifying a very low permeability along lines one gridpoint in thickness and 4 km in length. Figure 4-6 shows the velocity vectors and several streamlines depicting the groundwater flow field directly beneath Yucca Mountain for the case of a single dike oriented N15°E. Based on the existing fracture and faulting pattern at Yucca Mountain, it is believed that this could be a likely orientation for a possible dike intrusion. Figure 4-6 shows that to the left of the dike, the flow field can be seen to be

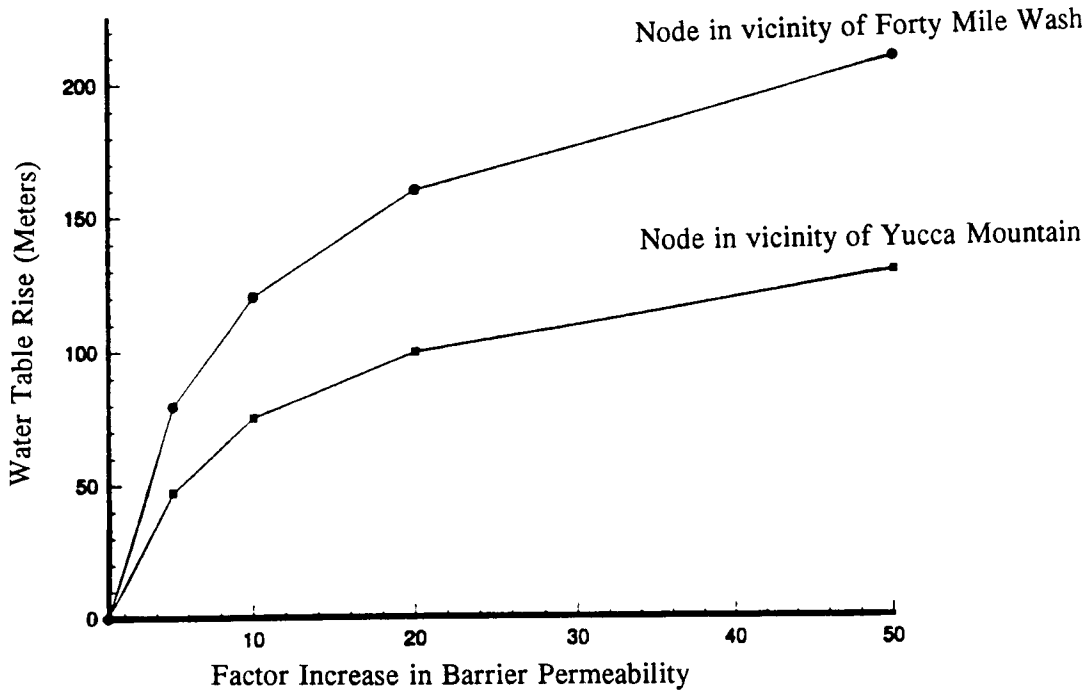

Figure 4-5. Water table rise at Yucca Mountain and Forty Mile Wash as a result of increasing the permeability through the barriers north and northeast of the site

directed towards the south. Around the lower tip of the dike, some of the flow is directed back to the north. Without the presence of the dike, the flow through this area is primarily east and southeast. The small circle in this figure indicates the location where the maximum water table rise occurred, which in this case was 79 m. Even though the groundwater travel time through the unsaturated zone would be somewhat decreased, the travel time in the saturated zone could be substantially increased, especially for the portion of the radionuclide inventory that entered the saturated zone on the left side of the dike. Figure 4-7 shows the numerical simulation results for the water table rise at the repository site for various dike orientations. The figure suggests that a dike oriented roughly north to northeast would produce the maximum water table rise for a single dike intrusion.

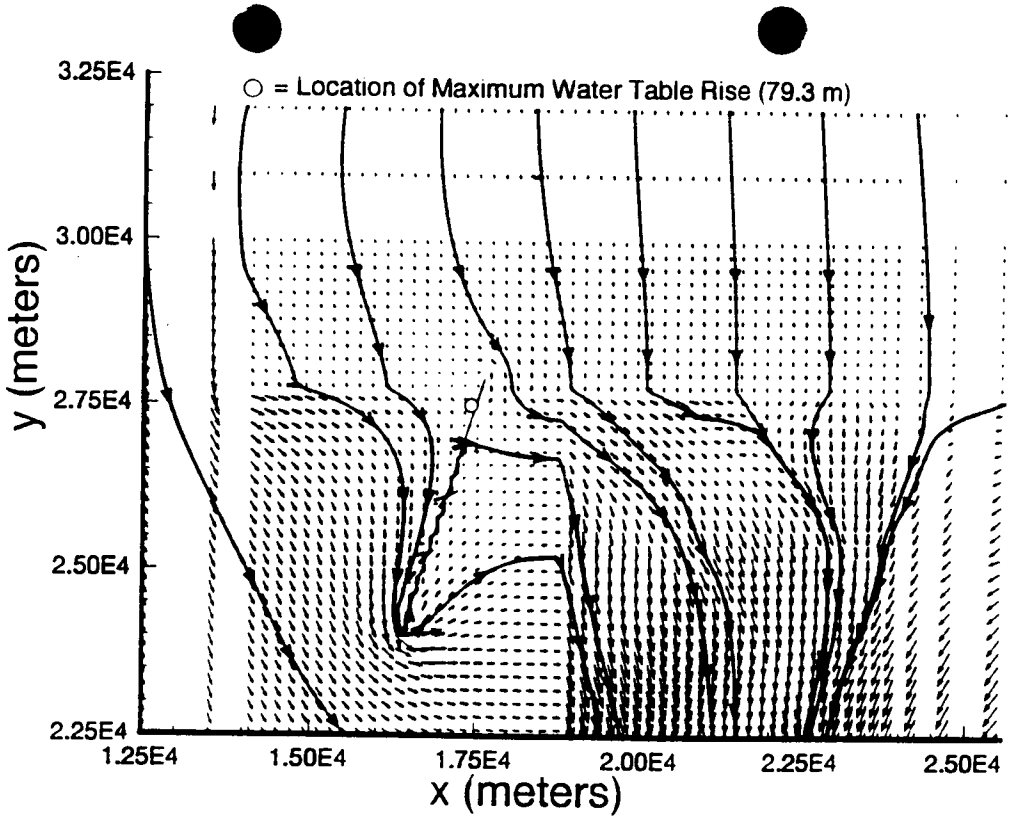

Figure 4-6. Impact of the intrusion of a single volcanic dike oriented N15°E on the groundwater flow field directly below the repository. The straight line indicates the location of the dike.

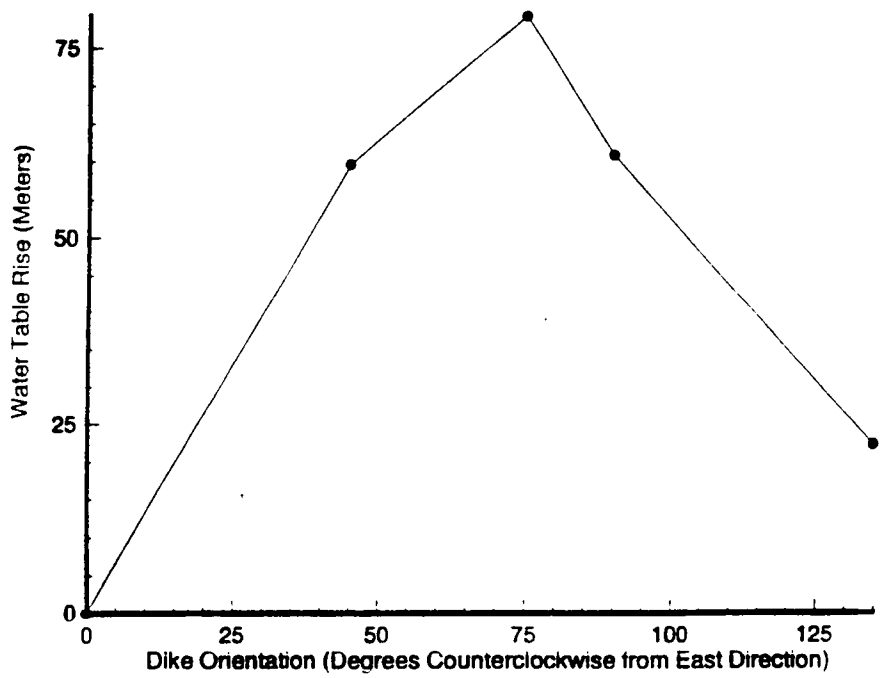

Figure 4-7. Maximum water table rise at potential repository site as a function of dike orientation

Figure 4-8 shows the intrusion of a second dike, which is perpendicular to the one shown in Figure 4-6. This case was simulated because it is believed to be not uncommon for volcanic dikes to occur in pairs at more or less perpendicular orientations. Interestingly, Figure 4-8 shows the dikes create stagnant pools of water which again may increase the length of the flow path in the saturated zone to the accessible environment. The maximum water table rise for this case of two perpendicular dikes was 103.4 m.

4.5.3.5 Summary of Conclusions

A summary of the results from both a regional and subregional groundwater-flow analysis of the saturated zone surrounding Yucca Mountain using the PORFLOW finite-difference code are presented. These results show the effects of various disruptive conditions on the water table elevations and resulting groundwater-flow directions near the proposed HLW repository. The results give an indication of what conditions would have a minimal impact on the saturated zone hydrology near the site, and those that would have a major impact. A rise in water table in the area of Forty Mile Wash was calculated to be greater than 200 m, based on certain disruptive conditions simulated using the regional model. Because evapotranspiration and surface runoff was neglected, the actual rise would be less than calculated. In addition, the subregional model analysis showed a rise in the water table near the repository ranging from a few meters to as much as 103 m, depending on the orientation of the simulated volcanic dikes.

The results presented here are meant to be preliminary and likely to change as site characterization studies at Yucca Mountain provide more accurate hydrological parameters and better information on which disruptive conditions would be more likely to occur in the future. Also, some of the assumptions in this analysis could be improved in future studies. For instance, with respect to the high water table rises predicted, the formation of new discharge areas that such a rise may cause was completely neglected.

4.5.7 Effects of Layering, Dipping, and Sub-Vertical Faults

4.5.7.1 Introduction

This section presents results of unsaturated flow simulations undertaken as an auxiliary analysis for the IPA project, one of the approaches adopted by the U.S. Nuclear Regulatory Commission (NRC) to develop repository license application review capabilities. The effects on flow of common geological features in a 2D domain, such as nonhorizontal stratification and vertical or near-vertical fault zones intersecting the strata, are of importance. In this work, numerical analysis is performed for a deep (approximately 530 m) hard rock system. The BIGFLOW numerical code (Bagtzoglou et al., 1992a) is used in these simulations. Some of the data (i.e., the depth to water table, the number of primary geologic strata, their dipping angle, and the existence of a fault zone) for the analysis were taken from the Yucca Mountain project reports (Scott and Bonk, 1984), but were adjusted to enhance the effects under study. In particular, extreme net infiltration rates (up to 50 mm/year) and hydraulic properties similar to the Calico Hills nonvitrified (CHnv) unit were considered. Therefore, conclusions regarding suitability of Yucca Mountain for the proposed HLW repository are not directly derivable from this analysis. Recognizing that there are no simple, natural initial-boundary conditions that can be used for the more complex problems, a method of successive approximation is implemented. This method uses solutions of auxiliary flow problems to set up pressure boundary conditions for the more complex

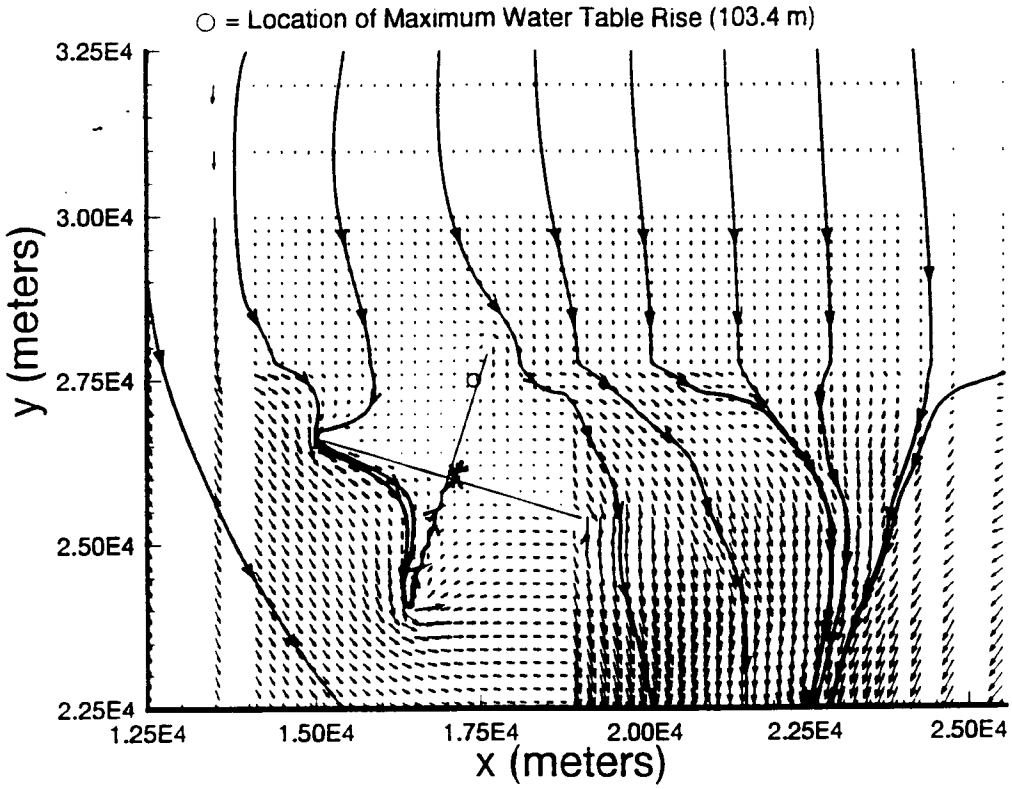

Figure 4-8. Impact of the intrusion of multiple volcanic dikes on the groundwater flow field directly below the repository. The straight lines indicate the location of the dikes.

problems. This is necessary because, in practice, no natural boundaries exist (or are adequately defined), especially in the lateral directions. The investigation is limited to three-dimensional (3D) simulations in a vertical, thin slice cross-section with dipping layers intersected by a subvertical fault zone. The simulations are performed in a transient mode to study the manner in which the solutions of the flow equation approach steady state. A "wet" hydro-climatic condition, in terms of perceived net infiltration rates, corresponding to a net annual infiltration rate of 50 mm/year is modeled. A hypothetical test problem is developed to study the effects of bedding, presence of a subvertical fault, and inclination of the beds.

The BIGFLOW simulation code accommodates 3D transient or steady flow in saturated, or partially saturated porous media with heterogeneous or spatially random hydrodynamic coefficients. For partially saturated flow, a mixed variable formulation of Richards' equation is used. That is

$$\frac{\partial \theta(h,x)}{\partial t} = \nabla \left[K\,(h,x)\,(\nabla h + g) \right] \tag{4-1}$$

where h is pressure head (m), θ is volumetric water content (m^3/m^3), K is hydraulic conductivity (m/s), and g is the body force unit vector aligned with, and opposed to, the acceleration of gravity. The differential equations are discretized by an implicit finite-difference scheme, two-point backward Euler in time, and seven-point centered in space. The spatial mesh is a regular rectangular lattice. The time step is generally variable and self-adjusted. The computational domain is a 3D parallelepiped, whose

coordinate system may be inclined at arbitrary angles with respect to the natural, horizontal-vertical coordinate system.

4.5.7.2 Description of Analyses

The hydrogeologic properties in the unsaturated zone of Yucca Mountain, Nevada, were considered in order to represent, to some degree, the general features of the site in the simulations. Yucca Mountain consists of a series of North-trending fault-block ridges composed of layers of volcanic ash tuffs that generally have a regional dip of 5° to 7° to the East (Scott and Bonk, 1984). The proposed repository area is also bounded by steeply dipping faults or by fault zones, and is transected by a few normal faults. Therefore, it is important to study the effects of layering, regional dipping, and fault zones on unsaturated water flow.

In the simulations presented herein, the computational domain is assumed to consist of five layers with approximately equal thicknesses spanning a total depth of 530 m at which depth the water table is assumed to be located. The computational domain used in these simulations is based on a 3D cartesian grid system. The axes of this system are aligned with East-West (X-axis), North-South (Y-axis), and vertical (Z-axis). The dimensions of the computational domain are 1230 m, 80 m, and 530 m in the X-, Y-, and Z-directions, respectively. The domain is discretized into $29 \times 5 \times 54$ nodes comprising a total of 7,830 nodes (Figure 4-9).

The functional forms of pressure-dependent hydraulic conductivity and water content used herein are the exponential Gardner model for K(h) and the van Genuchten model for θ(h). The exponential conductivity model is

$$K(h) = K_s \exp\left[\alpha(h - h_b)\right] \qquad if\ h \le h_b$$
$$K(h) = K_s \qquad if\ h > h_b \tag{4-2}$$

where K_s is the saturated hydraulic conductivity, α is a characteristic inverse length scale or capillary diffusivity (Ababou, 1991), h is the pressure, and h_b is the air-entry pressure. The van Genuchten model for the retention curve is

$$\theta(h) = \theta_r + (\theta_s - \theta_r)\left[1 + (-\beta h)^n\right]^{-m} \tag{4-3}$$

where θ_s and θ_r are the saturated and residual moisture contents, respectively, β is a characteristic inverse length (similar to α in Eq. 4-2), and n and m are real exponents (dependent upon distribution of pore sizes) related by the Mualem constraint.

All of the parameters in Eqs. (4-2) and (4-3) are, generally, spatially varying functions in all three dimensions. In the present work, however, they are assumed to be constant within a layer. Furthermore, the layer properties (K_s, α, h_b, and β) are assumed to be interchanging log-deviations around the geometric mean of each respective parameter [$\omega_G \exp(\pm\ \sigma_{ln\omega})$], taken herein as representative of the CHnv unit. The remaining matrix parameters are assumed to be constant in all layers, and are assigned typical values of the CHnv unit. Thus, θ_s = 44.11 percent, θ_r = 1.89 percent, n = 3.872, and m = 0.7417. The fault was arbitrarily modeled as a three-cell wide, YZ-planar zone located in the middle of the domain. Table 4-2 summarizes the hydraulic properties discussed above for the matrix

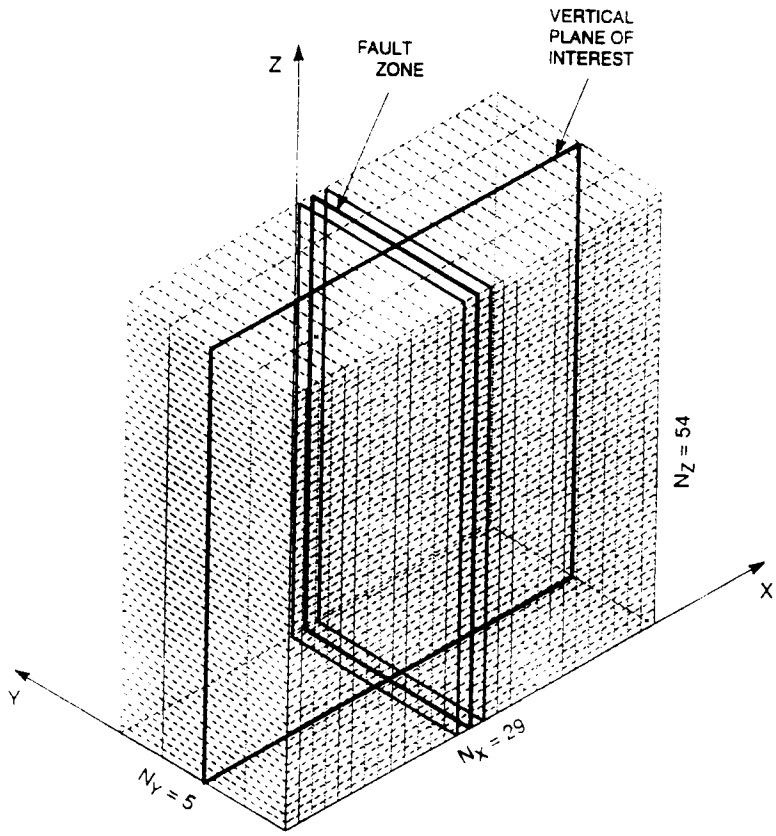

Figure 4-9. Computational grid

layers and fault zone.

The values of these parameters, when substituted in Eq. (4-2), yield different types of pressure-dependent curves K(h). It is worthwhile noticing that the fault hydraulic conductivity is much greater than the matrix hydraulic conductivity near saturation, and remains higher for values of suction head up to about 50 m. On the other hand, the fault becomes less conductive than the matrix for values of suction head significantly higher than 50 m. The existence of a crossing point, where the fault becomes less permeable than the matrix, is of particular interest and, as will be shown later in this work, directly

Table 4-2. Values of Spatially Variable Hydraulic Parameters

Parameters	K_S (m/d)	α (m^{-1})	h_b (m)	β (m^{-1})
Geo.Mean ω_G	2.33×10^{-2}	2.2×10^{-2}	20	5×10^{-2}
Std.Dev. $\sigma_{\ln\omega}$	1.0	0.2	0.2	0.2
Fault Zone	9.32×10^{-1}	1.0×10^{-1}	10.417	9.6×10^{-2}

affects the overall behavior of the flow system. When parameter α_f is reduced threefold, a crossing point at a higher value of suction, ψ = 260 m is attained. Note that, in terms of conductivities, this corresponds to a fault which is more like the porous matrix. Even though parameter β is varied from matrix to fault region, the remaining moisture retention curve properties are kept constant causing the fault to desaturate at smaller suctions than the porous matrix.

The regional dip (6° to the East) results in an approximately 10 percent fraction of the body (gravity) force being parallel to the X-axis attached to the dipped domain. Finally, the net infiltration rate q_o is taken to vary from 0 to 50 mm/year. In particular, the low value $q_o=0$ is used as a minimal base case, while the high value $q_o=50$ mm/year accounts for potential occurrence of extreme infiltration conditions.

4.5.7.3 Analyses Results and Discussion

Figure 4-10 depicts the temporal variation of the vertical pressure head profile, at the central transect Y = 40 m, X = 615 m, under a net infiltration rate of $q_o=1$ mm/year. It can be seen that steady-state is obtained only after 250 years of simulation. It is also apparent that the steady-state solution is much drier than the assumed (linear, but not hydrostatic) initial condition (deduced and modified from saturation values given by Montazer and Wilson, 1984), emphasizing the need for consistent initial and boundary conditions as discussed before. It can be observed, further, that the effect of stratification in hydraulic properties is felt only during the early times of simulation. However, due to the continuous influx of water from the top boundary, a nonhydrostatic pressure head profile is attained. The infiltration affects only the pressure profile in the coarse top layer. Finally, for the extremely wet case (q_o = 50 mm/year), the behavior of the flow system changes drastically. Steady-state flow conditions are attained faster, that is, after only 100 years of simulation. Figure 4-11 presents the temporal variation of the pressure head profile at the vertical transect (Y = 40 m, X = 615 m). For this simulation the initial condition is assumed to be hydrostatic. It is also worthwhile noticing that the effect of layering on pressure distribution appears to be almost insignificant for this flow rate, although the influence of the coarse top layer is still perceptible. Following a successive approximation methodology, the initial and boundary conditions for the simulations presented here are taken from the steady-state results of less complex flow systems. Figure 4-12 depicts results of a simulation with q_o = 50 mm/year, and a dipping angle of 6° to the East, at time t = 120 years, at vertical transects at three different locations within the flow domain. The effects of infiltration are felt by a region having the same lateral extent as in the previous simulations (about 100 m on either side of the fault). The infiltration "signal", however, is affecting a greater depth, down to almost 400 m. It is also shown that the effects of dipping are minor (less than 5 m of pressure head difference) for the conditions assumed in this analysis.

The high contrast in hydraulic properties between the matrix and fault zones renders the simulations extremely sensitive to the time step used. Choosing a $\Delta t_{max}=365$ days, for example, resulted in a nonbinding constraint for the time step. Even though the actual time step had an upper envelope of $\Delta t \approx 20$ days, mass balance errors as high as 20 percent were observed. This resulted in solutions that do not reach steady-state following an oscillatory pattern. When the lateral boundaries were set to no-flow (i.e., a 2D system), the mass balance error caused slight fluctuations of the total discharge rate on the order of 2 percent. This was in contrast with the more pronounced fluctuations obtained for a system with the fault cutting Dirichlet boundaries. It was found that in order to obtain a well-behaved numerical solution, with clearly stable convergence to steady-state, the time step had to be drastically reduced. When the maximum time step was decreased to Δt_{max} = 10 days, the mass balance plots indicated a complete elimination of large mass balance errors (except for early transients). The conclusion in this

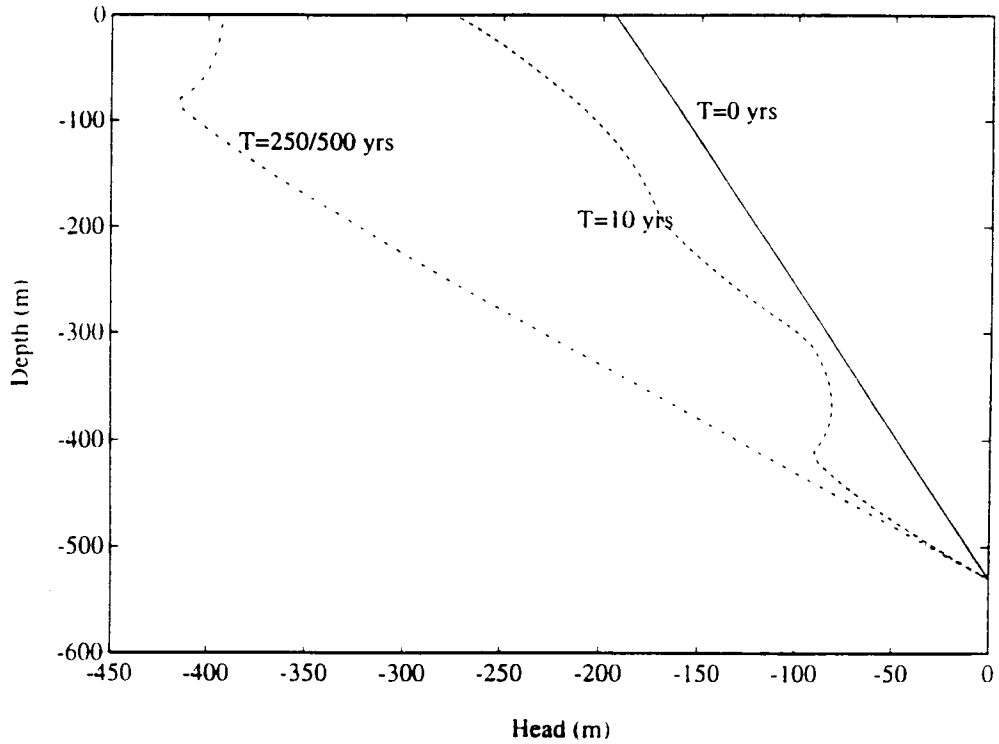

Figure 4-10. Pressure profiles for $q_0 = 1$ mm/year

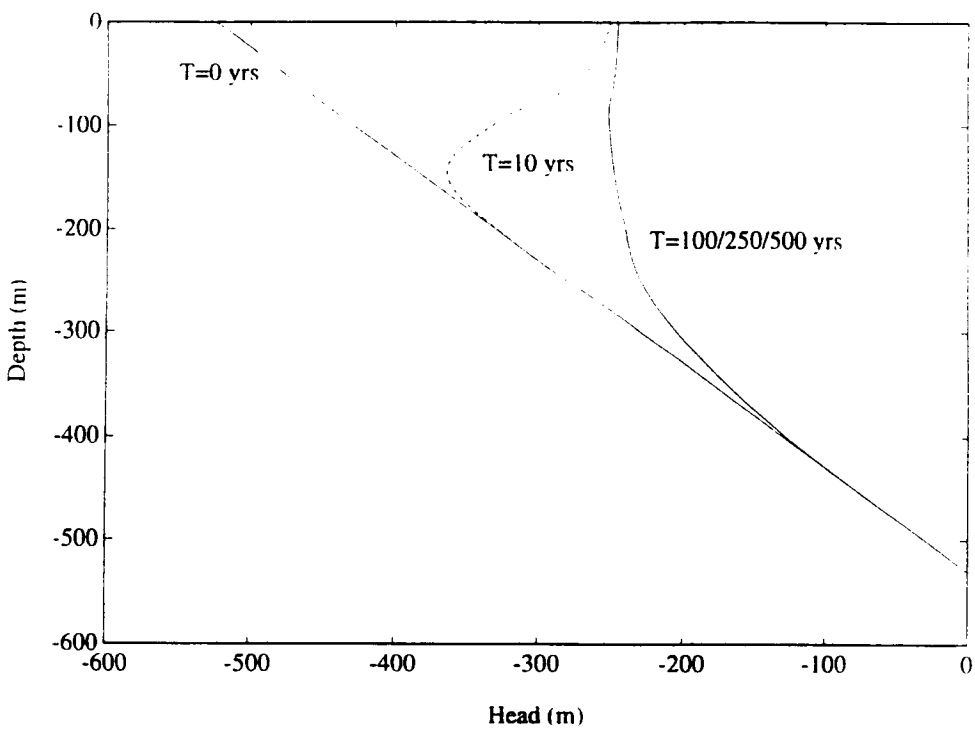

Figure 4-11. Pressure profiles for $q_0 = 50$ mm/year

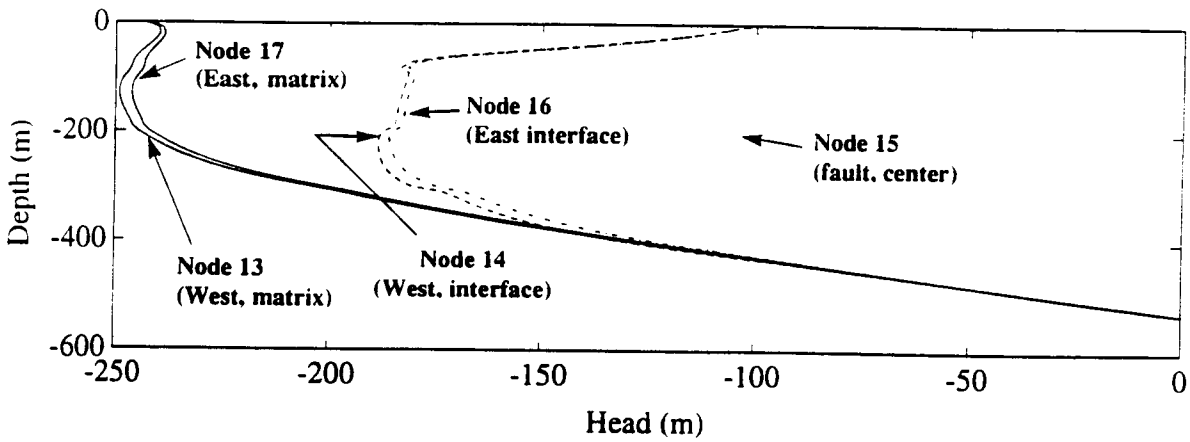

Figure 4-12. Pressure profile at t=120 yrs for q_0=50 mm/year and a dipping angle of 6^0

case was that, while the discrete-time system was unstable, the continuous-time system corresponding to a vanishingly small time step ($\Delta t \rightarrow 0$) is, in fact, stable and leads to a unique steady-state solution as $t \rightarrow \infty$. While this phenomenon results from the discreetness (in time) of the numerical flow problem, it indicated a peculiar phenomenon related to the 3D configuration of the faulted domain and to the direct connection between fault and permeable boundaries.

The steady-state flow pattern in each case is best represented by 2D vector plots of the unsaturated water velocity (or flux), and particle tracks depicting the locations of particles released in the steady flow system at selected points. These 2D vector and particle tracks are shown in Figures 4-13a and 4-13b for the higher and milder property contrast case, respectively. Inspection of these figures clearly shows a significant effect of the contrast between slopes of the matrix/fault unsaturated conductivities. When the fault's conductivity slope is comparatively much larger than that of the matrix (α_m = 0.022 m^{-1}, α_f = 0.10 m^{-1}), we observe higher fluxes in the matrix. This results in a front that lags within the fault zone. Figure 4-13(a) shows this effect for two lines of particles released at elevations 500 m and 300 m, respectively, and tracked for 1,000 years. In this case, the maximum distance traveled in 1,000 years is approximately 67 m. When the contrast is milder (α_m = 0.022 m^{-1}, α_f = 0.035 m^{-1}), the opposite behavior is observed. The fluxes within the fault zone are greater, but they point towards the matrix [Figure 4-13(b)]. This creates a frontal shape that continuously expands outward from the fault zone. In this case, the maximum distance traveled in 1,000 years is 165 m and more than 200 m, for the two release planes, respectively. This important difference in behavior is due to the different values of the crossing-point suction in the two cases. Recall that the contrast between matrix and fault moisture retention curves was not changed. As a consequence, the steady-state moisture patterns above the water table are almost identical for the two contrast cases studied. What is important to keep in mind is that the travel time of particles is sensitive to the unsaturated conductivity slope, even when the moisture retention curve is held constant.

4.5.7.4 Summary of Conclusions

A hypothetical test problem was developed in order to study the effect of bedding on flow, the presence of a subvertical fault zone, and the effect of inclination of the beds. A number of auxiliary tests

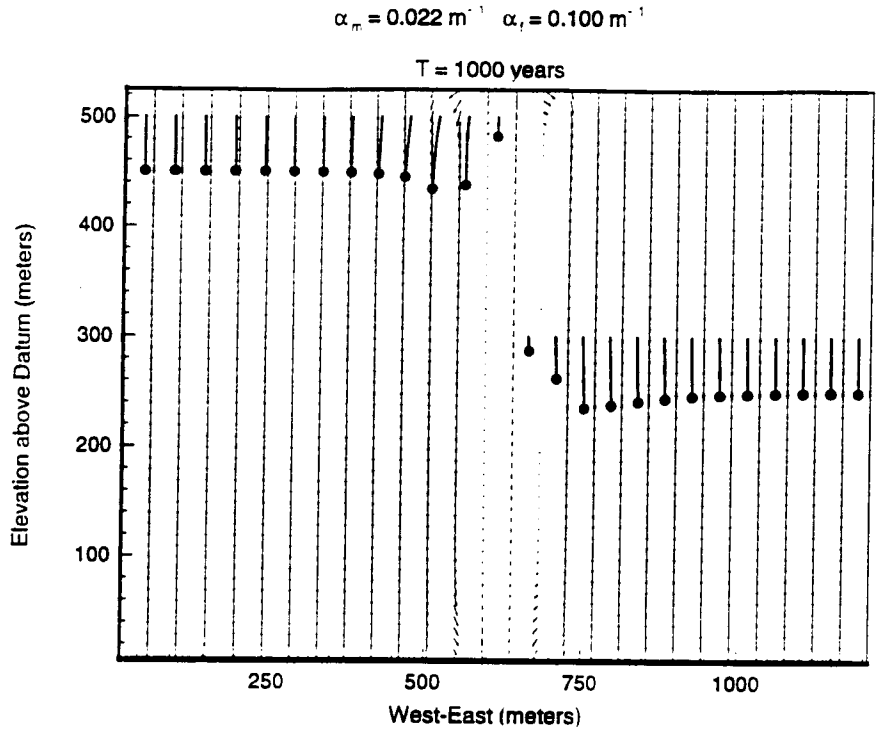

a)

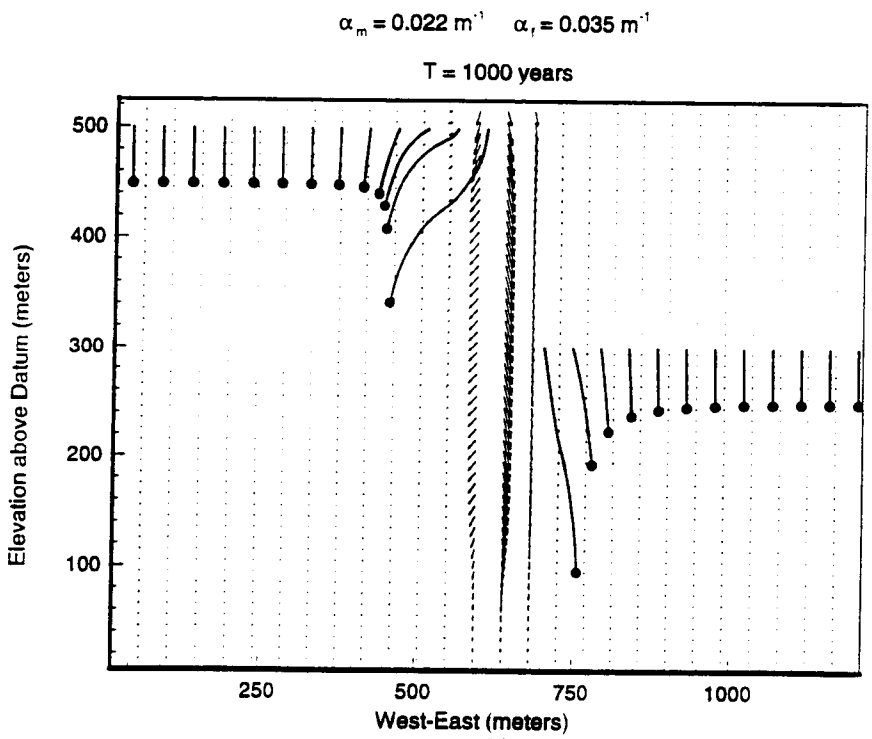

b)

Figure 4-13. XZ plane flux vector and particle plot: a) α_f = 0.1 m^{-1}; and b) α_f = 0.035 m^{-1}

were also conducted using variations on these hypothetical data. There are some similarities between this hypothetical problem and the Yucca Mountain stratigraphy, but since all site properties are not used, these simulations are not representative of the Yucca Mountain flow conditions.

Recognizing that there may not be natural initial-boundary conditions that can be used for the more complex problems, a method of successive approximation was implemented. This method uses solutions of auxiliary flow problems to set up pressure conditions for more complex problems. An oscillatory flow regime was observed at large times, that is, after initial transients died out. This was shown to be an effect of the discrete-time nature of the equations being solved, and was eliminated by using extremely small time steps ($\Delta t \rightarrow 0$). The techniques used to identify these effects relied on detailed plots of global mass balance in terms of instantaneous net discharge rate and instantaneous rate of change of total mass. Large Δt yielded oscillations for both 2D and 3D flow systems, but seemed more consequential in 3D (fault cutting pressure boundaries).

Based on the parameters used, and the simulations performed in this study the following conclusions can be reached:

- The effects of stratification are important only for low net infiltration rates ($q < 5$ mm/yr) and during the early parts of transient simulations ($t < 250$ yrs).

- A dipping angle of 6° to the East has a minimal effect on the pressure head distributions (approximately 2 percent of the maximum pressure head difference).

- The flow behavior (groundwater fluxes and travel times) of a system consisting of highly contrasted matrix and vertical fault properties (i.e., fault saturated conductivity equal to 40 times the geometric mean of the matrix saturated conductivity layers) is greatly influenced by the ratio of the slopes of the matrix and fault unsaturated hydraulic conductivity curves (as evidenced by changing the ratio from 4.54.to 1.59).

4.6 REFERENCES

Ababou, R. 1991. *Approaches to Large Scale Unsaturated Flow in Heterogeneous, Stratified, and Fractured Geologic Media.* NUREG/CR-5743. Washington, DC: U.S. Nuclear Regulatory Commission.

Ahola, M.P., and B. Sagar. 1992. *Regional Groundwater Modeling of the Saturated Zone in the Vicinity of Yucca Mountain, Nevada.* NUREG/CR-5890. Washington, DC: U.S. Nuclear Regulatory Commission.

Bagtzoglou, A.C., R. Ababou, and A. Nedungadi. 1992a. *BIGFLOW: A Multi-Dimensional Code for Flow in Heterogeneous and Variably Saturated Geologic Media (Theory and User's Manual - Version 1.0), CNWRA 92-026,* San Antonio, TX: Center for Nuclear Waste Regulatory Analyses: 140.

Bagtzoglou, A.C., R. Ababou, and B. Sagar. 1992b. *Effects of Layering, Dipping Angle, and Faulting on Two-Dimensional Variably Saturated Flow.* CNWRA 92-004. San Antonio, TX: Center for Nuclear Waste Regulatory Analyses.

Bear, J. 1972. *Dynamics of Fluids in Porous Media.* New York, NY: Dover Publications, Inc.: 764.

Czarnecki, J.B. 1985. *Simulated Effects of Increased Recharge on the Groundwater Flow System of Yucca Mountain and Vicinity, Nevada-California.* USGS-WRI-84-4344:33, Water Resources Investigations Report. Denver, CO: U.S. Geological Survey.

Czarnecki, J.B., and R.K. Waddell. 1984. *Finite-Element Simulation of Groundwater Flow in the Vicinity of Yucca Mountain, Nevada-California.* USGS-WRI-84-4349:38, Water Resources Investigations Report. Denver, CO: U.S. Geological Survey.

Montazer, P., and W.E. Wilson, 1984. *Conceptual Hydrologic Model of Flow in the Unsaturated Zone, Yucca Mountain, Nevada.* USGS-WRI-84-4345, Water Resources Investigations Report. Denver, CO: U.S. Geological Survey: 55.

Rice, W.A. 1984. *Preliminary Two-Dimensional Regional Hydrologic Model of Nevada Test Site and Vicinity.* SAND83-7466. Albuquerque, NM: Sandia National Laboratories: 44.

Runchal, A.K., and B. Sagar. 1989. *PORFLOW: A Mathematical Model for Fluid Flow, Heat, and Mass Transport in Variably Saturated Geologic Media - Users Manual, Version 1.0.* WHC-EP-0041. Richland, WA: Westinghouse Hanford Company.

Sagar, B., and A.K. Runchal. 1990. *PORFLOW: A Mathematical Model for Fluid Flow, Heat, and Mass Transport in Variably Saturated Geologic Media - Theory and Numerical Methods, Version 1.0.* WHC-EP-0042, Richland, WA: Westinghouse Hanford Company.

Scott, R.B., and J. Bonk. 1984. *Preliminary Geologic Map of Yucca Mountain with Geologic Sections, Nye County, Nevada.* U.S. Geological Survey Open-File Report 84-494.

U.S. Department of Energy (DOE). 1988. *Site Characterization Plan: Yucca Mountain Site, Nevada Research and Development Area.* Washington, DC: Department of Energy: II(3).

Waddell, R.K. 1982. *Two-Dimensional, Steady-State Model of Ground Water Flow, Nevada Test Site and Vicinity, Nevada-California.* USGS-WRI-82-4085:72, Water Resources Investigations Report. Denver, CO: U.S. Geological Survey.

Waddell, R.K., J.H. Robison, and R. K. Blankennagel. 1984. *Hydrology of Yucca Mountain and Vicinity, Nevada-California: Investigative Results Through Mid 1983.* USGS-WRI-84-4267:72. Water Resources Investigations Report. Denver, CO: U.S. Geological Survey.

5 SOURCE TERM MODULE

5.3.1 Corrosion Models

Calculation of waste package failures due to initial defects, corrosion, mechanical processes, and disruptions are considered. For corrosion processes, the corrosion potential is the master variable. For any given metal and set of environmental conditions, the corrosion potential determines the types of active corrosion processes (e.g., pitting, crevice, and general) and their associated rates. The importance of the corrosion potential as a master variable is reflected in the philosophy and implementation of the corrosion routines in SOTEC. The current version of SOTEC assumes that the corrosion potential is a function of temperature and radiation dose rate. The corrosion potential is computed from

$$E_{corr} = E_1 + A(T-298) + \beta e^{-\lambda t} \tag{5-1}$$

where

A	=	empirical factor for temperature effect on corrosion potential (mV/K)
β	=	empirical factor for radiolysis effect on corrosion potential (mV)
λ	=	average decay rate for gamma emitters in waste (yr^{-1})
E_1	=	reference corrosion potential (mV)
T	=	temperature (Kelvin)
t	=	time (yr)
E_{corr}	=	corrosion potential (mV)

The above equation for the corrosion potential assumes that the influence of radiolysis varies linearly with gamma dose rate and that temperature affects the corrosion potential in a linear fashion. The impact of radiolysis appears at time = 0, and declines with time with radioactive decay of gamma emitters. The dependence of the corrosion potential on temperature and radiolysis is presumed to be obtained from independent theoretical analysis (e.g., Macdonald and Urquidi-Macdonald, 1990) or experimental data and translated into functional forms allowed in SOTEC.

Rates of pitting and crevice corrosion depend directly on the corrosion potential. Localized corrosion begins when the potential is elevated above a critical value which is dependent upon the metal, metal history, and solution composition. The critical potential may be referred to as E_{pit}, E_{crev}, or E_{crit} depending upon the context and the type of corrosion involved. When the potential is lowered sufficiently, the localized corrosion cavities generally repassivate. This is sometimes referred to as the repassivation potential or protection potential E_{prot}.

SOTEC currently allows only one critical potential for each of pitting and crevice corrosion and the critical potential is assumed to be a function of temperature but not of solution composition. These expressions for the critical potential will be expanded in future versions of the code.

5.3.1.1 General Corrosion

General corrosion is assumed to begin when repository temperatures drop below a specified (input) temperature. In the atmosphere, general corrosion is known to become significant when the

relative humidity exceeds 80 percent. At the elevation of Yucca Mountain, this corresponds to a temperature of approximately 98°C assuming conservatively that the air is 100 percent water vapor. Once corrosion begins, the corrosion rate is described by a generic power law equation (for more discussion, see Williford, 1991) of the form:

$$r = ae^{\frac{b}{cT}} t^d C_1^e C_2^f \qquad T < T^\circ \tag{5-2}$$

where

r	=	corrosion rate
a,b,c,d,e,f	=	empirical constants
T	=	absolute temperature
t	=	time

Instead of concentrations C_1, C_2, etc., of aggressive species, the logarithm (to base 10) of the concentrations can be used. In some interpretations of this equation (e.g., Kubaschewski and Hopkins, 1962), b is the activation energy, and c is the gas law constant.

General corrosion is assumed to represent a passivated metal and as such is independent of the corrosion potential.

5.3.1.2 Crevice Corrosion

Crevice corrosion is affected by a number of coupled processes. These include mass transfer, production of metal ions within the crevice, and hydrolysis. In the literature both the steady-state and transient models for crevice corrosion exist (see Watson and Postlethwaite, 1990 as an example). However, for inclusion in SOTEC, such models are too complex and computationally time consuming. A strategy to develop a simple parametric equation for crevice corrosion for use in SOTEC has been adopted. In the future versions of SOTEC, the parametric equation will be based on the results of complex physics-based models.

Crevice corrosion has two characteristics, initiation time and propagation rate. Initiation time is dependent upon the corrosion potential of the metal exceeding the critical potential for crevice corrosion initiation. After the critical potential is exceeded, an additional period of time is required for destruction of the passive film in the crevice leading to active corrosion. The current version of SOTEC conservatively ignores crevice corrosion initiation time. For small crevices, the initiation time will be very short relative to the time scales of interest for waste isolation. For crevice geometries of a very large size, the initiation time may be of significance but will be difficult to predict with high confidence.

The repassivation potential is taken to be a function of temperature.

$$E_{rc} = E_r + \zeta T \tag{5-3}$$

where

E_{rc}	=	crevice repassivation potential (mV versus SHE)
E_r	=	reference potential (mV)
ζ	=	temperature correction factor (mV/K).

Subsequent to initiation, crevice corrosion is assumed to penetrate the container at a constant empirical rate, r. The active corrosion rate can be estimated from an equation of the form:

$$r = \frac{i_a w}{\rho z F} \tag{5-4}$$

where

i_a = active current density, w is the formula weight of the material, ρ is the material density, z is the ion valency, and F is the Faraday constant. SOTEC assumes a constant active corrosion rate.

5.3.1.3 Pitting Corrosion

Episodic evaporation and condensation of water on the surface of waste containers resulting in high concentration of aggressive ions makes them susceptible to pitting corrosion. Mechanistically, pitting corrosion is similar to crevice corrosion, and it is possible to develop detailed models (Farmer et al., 1991) for predicting critical pitting potentials or electrochemical conditions within the pit. Alternatively, heuristic stochastic models may also be developed (Henshall, 1991). For development of the SOTEC code, a strategy similar to that for crevice corrosion will be followed. Detailed models for pitting corrosion are still under development, and a constant propagation rate is assumed for pitting in Version 1.0 of SOTEC.

Pitting corrosion is assumed to begin when the critical potential for pitting is reached. The initiation time for pitting is assumed to be very short relative to the time frame of interest, thus pitting is assumed to begin immediately when the critical potential is exceeded. The critical potential is given by Eq. (5-3). The rate of penetration by pitting is assumed to be identical to the rate in crevice corrosion as described by Eq. (5-4).

5.6 OVERALL STRUCTURE OF THE SOURCE TERM CODE

5.6.1 Conceptual Model

The proposed repository at Yucca Mountain is designed to contain a large number of waste packages placed in drifts and perhaps in boreholes. The repository environment will change with time as a result of radioactive decay leading to initial heating of the rock followed by a long cooling period. The heating is anticipated to promote significant changes in the chemical and hydrologic environment surrounding the waste containers. Temperature and water flow rates will vary widely over the spatial scale of a repository. The geology of the mountain is of a fractured, porous rock material with high spatial variability. The problems with heterogeneity are increased because the type of water flow of greatest concern is fracture flow. The characteristics of the waste material such as age, burnup, heavy metal inventory, and spent fuel versus glass will vary spatially in the repository. Environmental variables such as water flow rates, water saturation, water chemistry, and temperature will vary in time and in space in the repository.

The problem of heterogeneity is addressed in SOTEC by dividing the repository into a number of cells or zones. Within each cell, all chemical, physical, and waste properties are assumed to be

identical. The release rate for each cell is then the release rate for an individual waste package in the zone times the number of waste packages in the cell. SOTEC calculates the performance characteristics for an individual waste container and extrapolates the result to the entire cell.

Information concerning variability may come either from standard input parameters or from output files created by other codes. In order to limit the amount of input data and code complexity, the assumption is made that (except for temperature) a separation of variables can be performed between spatial and temporal variations. For each parameter, the input appears as a time variant repository average (or reference) value and a set of load factors for the individual cells. The load factors vary among the cells and are specified in the input deck. The separation of variables is analogous to many analytical solutions for partial differential equations where spatial and temporal variability can be separated mathematically. In SOTEC the separation of variables is made for convenience. The one exception to the load factor concept is temperature. Separate time histories for temperature are read into each repository cell. This is done for reasons of compatibility between SOTEC and the temperature code. The present versions of SOTEC and the temperature code consider only 7 or 17 separate cells in the repository. The small number of cells is inadequate to describe a continuous distribution of container failure times and Engineered Barriers release rate.

5.6.2 Input and Output Files

The structure and flow of the source term code is illustrated in Figures 5-1 and 5-2. Data are read into SOTEC from a series of files. Some of the file names are initially fixed, however the majority of file names are read from the main input files. Files with flexible naming are placed in "quotes" in the discussion and figures. The main input file for SOTEC is sotec.inp. The file "flosot.dat" contains water flow rate data from the FLOWMOD code. Temperature versus time histories from the CANT2 code are read from the file "tzone.dat" and radionuclide specific data is read from the file "sotec.nuc". Depending upon the scenario being considered in Total Performance Assessment (TPA) mode, the "seisot.dat" file from SEISMO and the drlsot.dat file from DRILLO may be read by SOTEC. Mechanical loads on the container are read in the file "mechan.dat."

The presence or absence of the file TPA_SOT.SGD determines whether the TPA mode is operational. If the file is absent, standalone mode is operational. If the file is present, total systems mode is assumed and the Latin Hypercube file is read ("lhs0000.out"). In TPA mode, many of the variables in SOTEC which are read from the standalone input files are overwritten. Overwritten variables represent either random variables or system wide input variables. Figure 5-1 presents input and output files for SOTEC. Some of the output files for SOTEC are only written when operation is in TPA mode.

All of the major output files written by SOTEC are designed to be read from other codes. Diagnostic output is sent to the default output unit, typically the screen. On Unix operating systems the diagnostic messages may be redirected to a file. The diagnostic output echoes the "sotec.inp" file, and prints a summary of container lifetime and normalized cumulative release numbers for each radionuclide released from each cell in the liquid or gas phase. This output is intended to assist the user with following the calculations and checking for abnormalities.

The file "sotnef.dat" provides the release rate as a function of time for each radionuclide for each cell to be read by NEFTRAN. This represents the major output file when running in TPA mode. Container lifetimes are output in the file confail.out. The file "inv1000.out" contains the 1,000-year

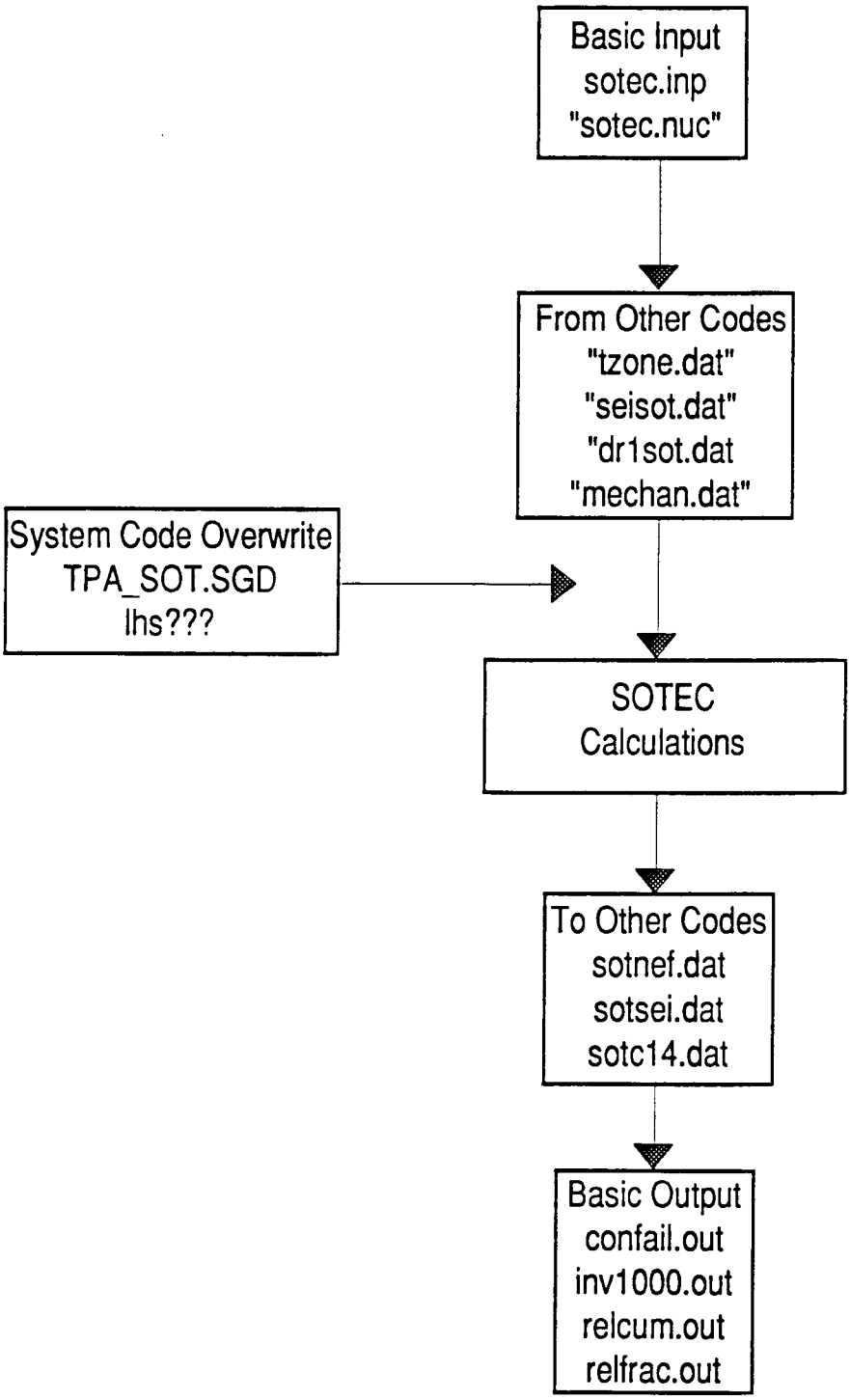

Figure 5-1. SOTEC code - relationship of input and output files

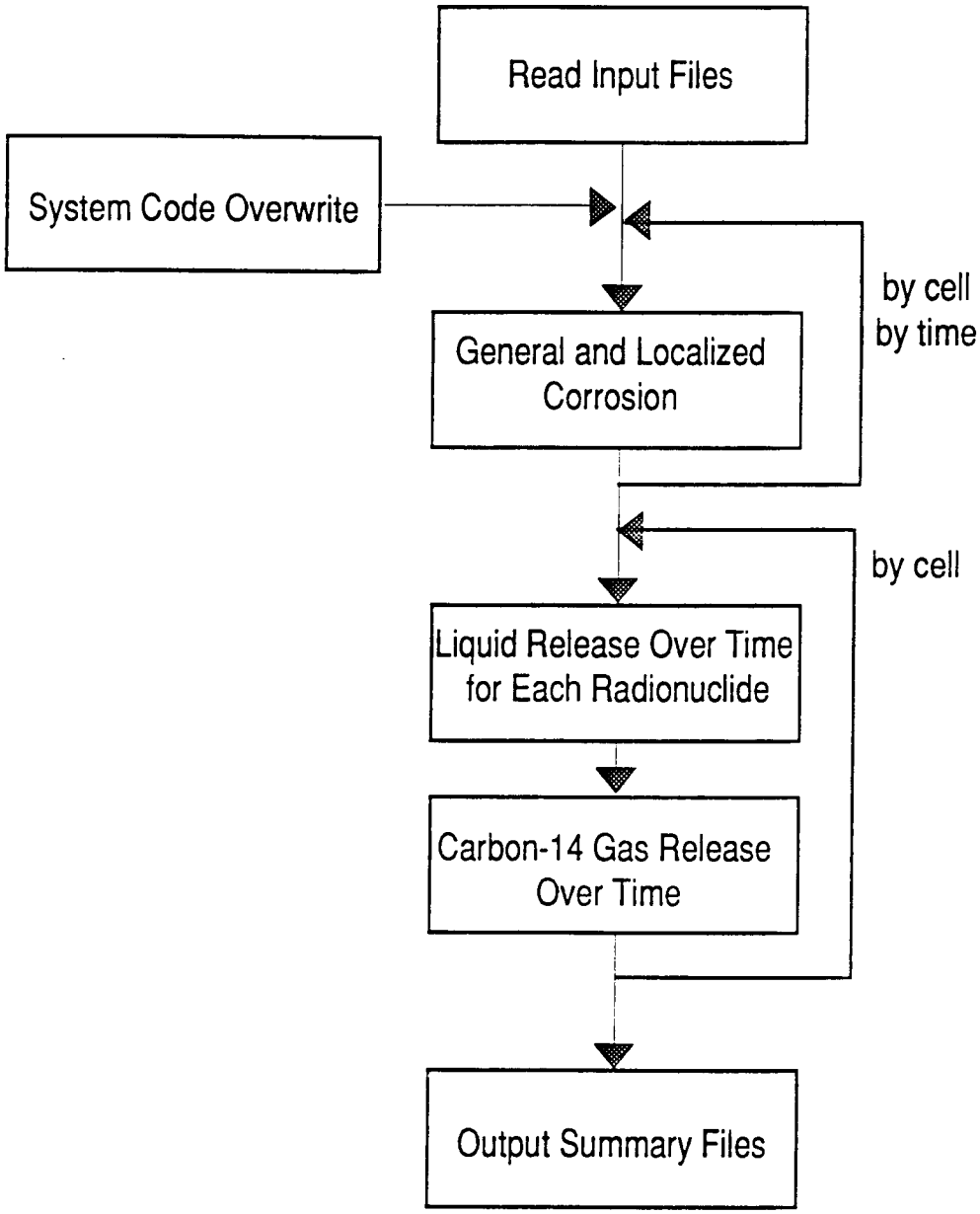

Figure 5-2. SOTEC - general flowchart

inventory for each radionuclide, assuming no leaching. This file may be useful for comparisons with the NRC release rate standard that requires normalization relative to the 1,000-year inventory. The file relcum.out is the cumulative release from the Engineered Barrier System (EBS) of each radionuclide in each cell. The file also contains the cumulative release normalized by the initial (i.e., at t=0) inventory for each radionuclide. The file "relfrac.out" provides the release rate of each radionuclide normalized by the 1,000-year inventory. No provision is made in the normalization for low inventory radionuclides as specified in the regulation. Carbon-14 releases as a function of time are output in the file "sotc14.dat".

In TPA mode, the file "sotsei.dat" is written to SEISMO. Depending upon the scenario being considered in TPA mode, the "seisot.dat" file from SEISMO and the "drlsot.dat" file from DRILLO may be read by SOTEC.

5.6.3 Structure of Calculations

The overall flow of the calculations in SOTEC is illustrated in Figure 5-2. Subsequent to reading the input files, SOTEC loops over time calculating corrosion penetration for each container as a function of time. Container failure times for each cell are recorded in variables for use in the release rate portion of the code. The corrosion portion of SOTEC is not coupled to the liquid release calculations and could, theoretically, be put in a separate code. In the corrosion calculations, the corrosion rate is estimated at the beginning of each time step and integrated with Euler's method. At the end of the time step, the total corrosion depth is compared with the critical thickness for buckling. If the remaining container thickness is less than the critical thickness, or if the remaining thickness is less than zero, failure is presumed to occur. Depending upon input assumptions, the container may either fail completely, resulting in a flow through system, or partially fail, leading to a bathtub configuration with a specified volume inside the remaining container. However, no additional degradation of the container is considered. A container that fails in a bathtub configuration will always retain the same bathtub configuration.

Calculation of liquid and gaseous releases begins with evaluation of the failure time and types for each cell. Individual waste containers in each cell can fail by three different mechanisms. The first type of failure is initial defectives. Initial defectives represent containers that were defective at the time of repository closure (e.g., by defective welds). Defective containers will begin releasing carbon-14 at time = 0 and begin releasing radionuclides in the aqueous phase when the container cools below the boiling point of water. The second type of failure is by scenario. The scenario option fundamentally allows the TPA code or the analyst to specify a time of failure for a portion of the containers in each cell. The primary purpose is to facilitate evaluation of alternative scenarios besides corrosion/buckling failure of the waste containers. The scenario option can also be used by the TPA code to specify a container lifetime distribution independent of the corrosion calculations. The third type of container failure is by the corrosion/buckling mechanism discussed above.

After sorting out the type and timing of the failures in each cell, the liquid and gaseous release calculations begin. The calculations proceed by cell with internal time and radionuclide loops in the liquid and gas release modules. The calculations are set up to handle multiple chains of radionuclides and multiple isotopes of the same element.

Subsequent to the release calculations, the release rates are summarized by calculating cumulative release and interpolated to even grids for writing to file.

5.7 REFERENCES

Farmer, J.C., G.E. Gdowski, R.D. McCright, and H.S. Abluwablia. 1991. Corrosion models for performance assessment of high-level radioactive-waste containers. *Nucl. Eng. Design* 129: 57-88.

Henshall, G.A. 1991. *Stochastic models for predicting pitting corrosion damage of HLRW containers.* Proceedings of FOCUS'91. American Nuclear Society: 8.

Kubaschewski, O., and B.E. Hopkins. 1962. *Oxidation of Metals and Alloys.* London, England: Butterworth Publishers: 36.

Macdonald, D.D., and M. Urquidi-Macdonald. 1990. Thin-layer mixed-potential model for the corrosion of high-level nuclear waste canisters. *Corrosion* 46(5): 380-390.

Watson, M., and J. Postlethwaite. 1990. Numerical simulation of crevice corrosion of stainless steel and nickel alloys in chloride solutions. *Corrosion* 46(7): 522-530.

Williford, R.E. 1991. *Uncertainties in Container Failure Time Predictions.* Mat. Res. Soc. Symp. Proc. 212: 335-342.

6.4 MAGMATIC SCENARIOS MODEL AND CODE

6.4.1 Introduction

This section describes scenarios of magmatic models and codes that have been used for the Iterative Performance Assessment (IPA). Magmatic scenarios are important for performance assessment (PA) because some repository material will be ejected onto the earth's surface if a magmatic event penetrates the repository during a volcano eruption (Valentine et al., 1992). Even in the absence of actual eruption of waste, subsurface magmatic effects can also affect the repository performance. In the case of intrusive events that occur within the repository block, dikes or sills below or in the repository horizon could affect the repository by producing hydrothermal processes or altering hydrology. Hydrothermal processes could cause rapid corrosion of waste packages and accelerate transport of radionuclides to the accessible environment by either liquid- or vapor-phase transport. The hydrologic properties of the dike itself may produce important changes in the long term flow of groundwater.

Field evidence shows occurrences of magmatic activity in the vicinity of Yucca Mountain extending back several million years. Within a radius of 30 km of the repository, twenty nine post-caldera basaltic vents can be identified in the Yucca Mountain region (Crowe, 1992). The dated age of these basaltic vents varies from approximately 9 Ma for the Paiute Mesa basalts to approximately 0.13 Ma for the Lathrop Wells cinder cone. The repository site is located within the area of most recent volcanism (AMRV), which included all vents less than 2.8 Ma in the region (Smith et al., 1990). The AMRV comprises a polygonal area extending from Lathrop Wells cone north to the Sleeping Butte center and east to the Buckboard Mesa. In another study, Crowe (1992) has identified a different area, the Crater Flat Volcanic Zone (CFVZ), comprising an area extending NNW from the Amargosa center to the Sleeping Buttes center. In this model, the CFVZ trends near, but not through, the site of the repository.

Probability models for future disruptive events at the Yucca Mountain site rely on the volcanic history of the region to estimate the expected recurrence rate of volcanism in the area (Crowe et al., 1982; Crowe, 1992; Ho, 1992; Margulies et al., 1992). These models implicitly assume that previous volcanic events occurred according to a homogeneous Poisson distribution. The estimated probability for the formation of new volcanic centers in the repository region varies from approximately 1.0×10^{-5} (Crowe et al., 1982) to 1.0×10^{-3} (Ho, 1992). Margulies et al. (1992) derived the recurrence rate from the number of vents within the AMRV, the area of the AMRV, and the time interval over which the vents have been active. They estimated the probability of a magmatic event at Yucca Mountain in the next 10,000 years to be about 1.7×10^{-5}. However, Crowe et al. (1982) and Margulies et al. (1992) may have obtained lower estimates because too few events were considered in their studies. By assuming an increasing recurrence rate in the NE-trending zones through the AMRV, Ho et al. (1992) obtained a much higher recurrence rate.

Two approaches have been used to model the volcanism consequences related to damage of the repository and release of waste. The first method involves development of a geometric model to estimate the amount of waste entrained in an ascending dike during both intrusive and extrusive events. In this model it is assumed that the amount of waste entrained is directly proportional to the size of the dike. In the second approach, the likely amount of waste entrainment is estimated by considering the proportion of shallow crustal xenoliths identified near the repository site and other cinder cones in the Great Basin. The basic premise in this approach is that the amount of waste entrained should be proportional to the

lithic fraction in scoria cones, should a basaltic eruption occur through the repository. We adapted the geometric approach to develop the magmatic scenarios model and code for the IPA.

It should be pointed out that the geometric approach tends to give a low estimate of total releases because of the effects of magma fragmentation and depressurization at the repository horizon. To be conservative, we have assumed that all radioactive waste affected by the dike will be released into air through the cinder cone for extrusive events. For intrusive events, only subsurface magmatic effects are considered.

6.4.2 Relevant Literature

The volcanic release probability at Yucca Mountain region during the lifetime of the potential repository has been studied by Crowe et al. (1982, 1983) and Crowe (1992). The volcanic release probability was examined in these studies as the product of three factors: (i) the probability that a volcanic event will affect the repository site; (ii) the temporal probability of a volcanic event; and (iii) the probable amount of release of radionuclides due to a volcanic event. Critical parameters in the consequence analysis, such as erosion depth, conduit shape, speed of entrainment, and total lithic fraction, are underestimated by this PA model.

The effects of volcanism on performance of the potential Yucca Mountain radioactive waste repository were studied by Valentine et al. (1992). They adapted the implicit assumption of the geometric model that the amount of waste entrained is directly proportional to the size of the dike. Valentine et al. (1992) then estimated the amount of waste entrained from the total volume of erupted lithics and the volume of repository intercepted by the dike.

Sheridan (1992) used Monte Carlo simulation to estimate the probability of occurrence of future volcanic dikes in the vicinity of Yucca Mountain. His model incorporates the geometric approach and addresses only the spatial probability of the various volcanic scenarios. In this model, the volcanic field defining the area in which dikes can occur is approximated by an elliptical outline. The centers of the dikes are distributed according to a bivariate Gaussian distribution centered in the middle of the volcanic field. The geometric parameters of dikes are specified by a mean value and a standard deviation. After each dike is located, the length and orientation are chosen from the Gaussian distributions specified by the mean and standard deviation. Because the location of dike centers and the dike geometry are generated independently, it is possible to have a dike field oriented in a different direction away from the orientation of the elongated volcanic field. This study sets upper bounds on the probability of intersection of dikes with the repository. Using this technique, Sheridan (1992) estimated that the worst case probability of a volcanic dike intersection with the repository in the next 10,000 years is between 0.001 and 0.01.

Using a Monte Carlo simulation approach, Margulies et al. (1992) estimated the areal extent that a basaltic or volcanic cone intercepts the repository given the occurrence of magmatic activity in the region near the repository. The magmatic events modeled were represented by planar geometrical figures. Cones were represented as disks, and dikes were represented as rectangles. The repository area and borders were represented realistically in the simulations. Based only on geometry, Margulies et al. (1992) obtained conservative estimates of the upper bound for radionuclide release by assuming that any radioactive waste intercepted by the magma would result in release of radionuclides to the accessible environment.

Because Margulies et al. (1992) assumed a homogeneous Poisson model for the occurrence of a magmatic event, the probability of magmatism was uniform in the simulation region in their study. The vent distribution in the Yucca Mountain area indicates cluster of vents, which was not taken into account by Margulies et al. (1992). From geologic evidence and theory, the probability of magmatism is unlikely constant in time in the vicinity of Yucca Mountain (Trapp and Justus, 1992). Important geological information, such as the temporal and spatial variation in the rate of magmatism, therefore, remains to be incorporated into the geometric approach of simulating magmatic events in the repository site.

6.4.3 Description of Modeling Approach

6.4.3.1 Introduction

The geometric approach used is an extension of the work by Margulies et al. (1992). In the geometric approach, Monte Carlo sampling was used to estimate the areal extent that a basaltic dike or a volcano cone intercepts the repository. From a probabilistic point of view, magmatic events are distributed in both space and time. For the purposes of IPA, an estimate of the probability of magmatism in the Yucca Mountain repository (over the next 10,000 years) is needed. Margulies et al. (1992) allowed for variations in rate of occurrence of magmatism as functions of time and space. The hazard posed by the emplaced waste changes in time, because of radioactive decay and because the radionuclides eventually may be dispersed in the geosphere.

Margulies et al. (1992) assumed that the number of magmatic events at the repository may be described by a homogeneous Poisson distribution. Therefore, the probability $P(n,t)$ of n magmatic events occurring within the repository perimeter, over a time period of [0,t], is given by

$$P(n,t) = \frac{[\mu(t)]^n \, e^{-\mu(t)}}{n!} \tag{6-1}$$

where $\mu(t)$ is the expected number of magmatic events in the time period [0,t]. The expected number of events $\mu(t)$ in a region with an area A is defined as

$$\mu(t) = r \, A \, t \tag{6-2}$$

where r is defined as the recurrence rate of magmatism per unit area per unit time for the region of interest during the time period of interest.

6.4.3.2 Simulation Procedure

In the Monte Carlo simulation, we consider a rectangular region surrounding the repository horizon. As shown in the simulation configuration of the repository (Figure 6-1), the repository is represented by a total of 17 rectangles. To obtain the simulation configuration of the repository, the outline of the perimeter of the proposed Yucca mountain repository has been traced from actual drawings. The rectangles are further grouped into seven zones according to the radionuclide initial inventory.

The simulation generates a volcanic event randomly in the simulated region. The volcanic event occurrence time is chosen randomly within the specified time period. The simulation chooses an

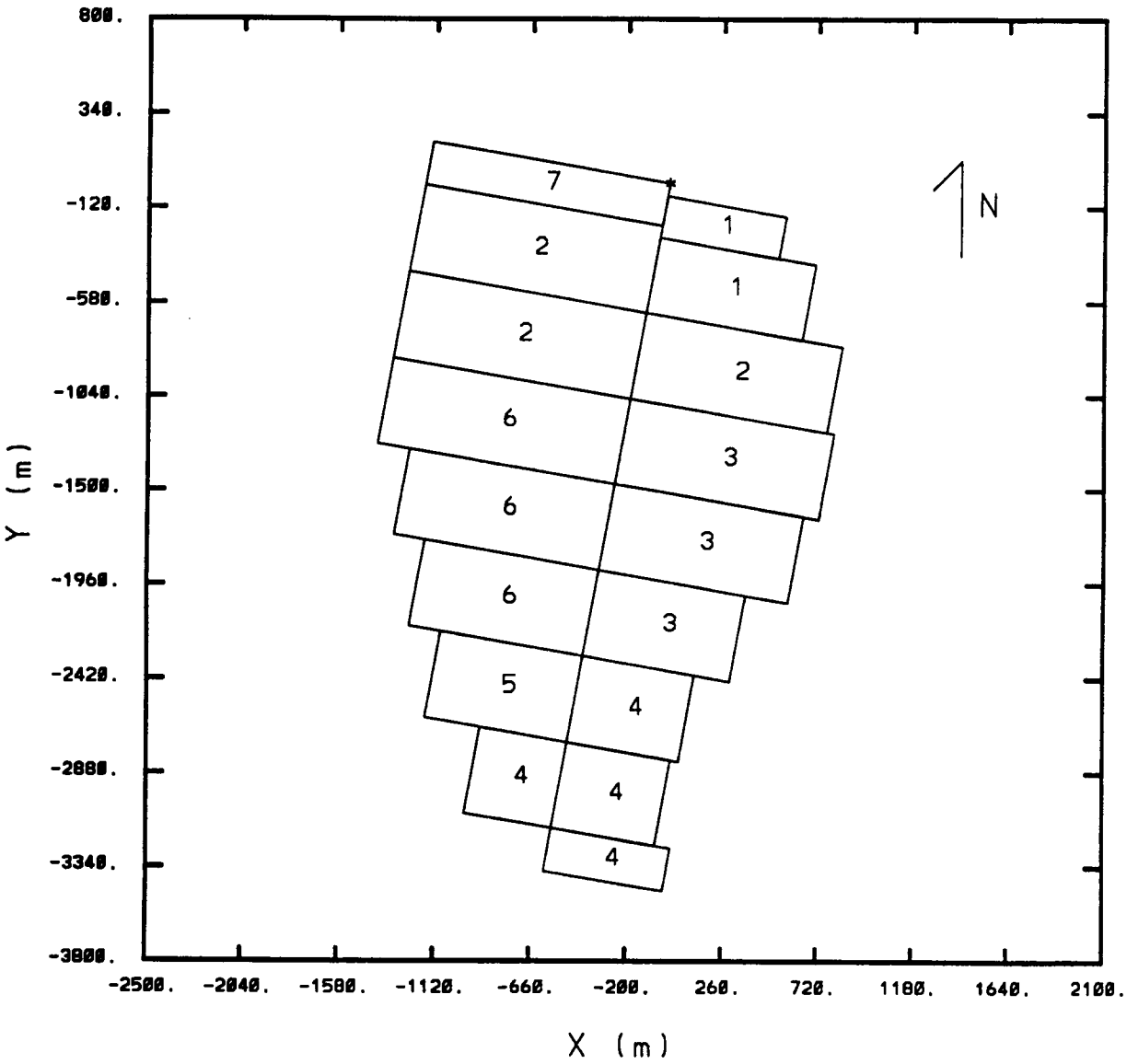

Figure 6-1. Configuration of the repository in the simulation. The repository is divided into 7 zones with a total of 17 rectangles. The number in each rectangle represents the zone number.

intrusive magma event (with only a dike) with a probability ten times that of an extrusive event (with a seeder dike and a cone). Cones are represented as circular disks, whereas dikes are represented as rectangles. The dimensions of cones and dikes are selected by a random sampling procedure. The Monte Carlo simulation procedure for estimating the occurrence and consequences of a magmatic event is described below:

- Locate a dike event or an extrusive event by random sampling

- Determine geometry parameters (e.g. length, width, radius) by random sampling
- Calculate the overlapped area in each repository zone and convert the area to number of waste containers, if a dike or a cone intercepts the repository
- Calculate and output the radioactive release amount in this trial

In the procedure of determining geometry parameters, parameters are chosen randomly from a range of values based on the available data. The available data suggest that the length of the rectangular dike ranges between 1,000 and 4,000 m, and the dike width ranges between 1 and 10 m. Therefore, the area of the rectangular dike varies between 1,000 and 40,000 m^2. The area of the rectangular dike is chosen at random in the code as given by the following expression:

$$A = a^{(1-\mu)} b^{\mu} \tag{6-3}$$

where a = 1,000 m^2 is the minimum area, b=40,000 m^2 is the maximum area, and u is a random number chosen uniformly between 0 and 1.

After the dike area is chosen, the length is chosen at random between max{c,A/f} and min{A/e,d} with equal probability. The corresponding width of the rectangular dike W is then determined from the area A and length L as W = A /L. Here the parameters c and d define the minimum and maximum length, respectively, whereas the parameters e and f define the minimum and maximum width, respectively. The values of these parameters in the code are:

c = 1,000 m (minimum length)
d = 4,000 m (maximum length)
e = 1 m (minimum width)
f = 10 m (maximum width).

This randomly generated rectangular dike has an angle of orientation that is chosen at random with equal probability between two angles specified in the input. Typically, the input parameters for the angles are chosen to be 75° and 90° counterclockwise from the horizontal axis, corresponding to the orientation of dikes in the direction ranging from north/south to 15 degrees to the east. However, this distribution of dike orientation is based on a postulate by Smith et al. (1990) and Ho et al. (1990) that there is a NE-trending structure control on vent distribution within the AMRV. Crowe (1992) has delineated a different zone, the CFVZ, that extends NNW from the Amorgosa center to the Sleeping Buttes center.

To simulate the formation of volcanic cones through extrusion events, circular areas are used to represent cones. Since we are interested in the effect of the volcano on the subsurface repository, these circular areas more properly represent the stem-like conduit of magma feeding the volcanic eruption, which may intersect the repository. The cone radius then corresponds approximately to the radius of the approximately vertical, nearly circular magma conduit. The radius of the volcanic cones is chosen uniformly at random between two input parameters, the minimum and maximum cone radii. Currently the simulation uses 25 and 100 meters for the minimum and maximum radii, respectively. However, it remains to be determined from geological data the realistic values of cone radius.

The simulation program calculates the area of intersection between the dike and the repository by strictly geometrical computations. For an extrusive event, it also calculates the area of intersection

between the cone and the repository. The predicted area of interception from the simulations is used to estimate the number of waste containers damaged, assuming a uniform distribution of waste containers within each repository zone. For extrusive events, upper bound and conservative estimates of radionuclide release into the atmosphere are calculated by assuming that the radioactivity material damaged by the dike has been transported to the cone and released to air. The amount of radionuclides released to air is considered to be zero for intrusive events.

The simulation estimates the amount of radioactivity release Q by each repository zone to the atmosphere for the extrusive event by summing over the radioactivity inventory of each radionuclide at the time of event,

$$Q = N_c \sum_k I_k(t) \tag{6-4}$$

where N_c is the number of the damaged waste containers and $I_k(t)$ is the inventory of *k*th radionuclide in each container at time t. The simulation output Q is in the unit of Curies. Using the input of initial inventory $I_k(0)$ and the half-life t_k of each radionuclide, $I_k(t)$ is calculated as

$$I_k(t) = I_k(0) \exp\left(-0.693 t/t_k\right) \tag{6-5}$$

This approach neglects decay products. The amount of radioactivity release for each radionuclide is used as input by the AIRCON program to calculate DITTY (Dose In Ten Thousand Years). In addition, the number of damaged waste containers predicted by the Monte Carlo simulation is used by the SOTEC program to determine the decay and release of waste in air and water.

6.4.3.3 Assumptions and Limitations

Several assumptions are implied the geometric approach to estimate the amount of waste entrained in an ascending dike. Some of these assumptions are discussed in Valentine et al. (1992), whereas others are not. The Monte Carlo simulation model of basaltic igneous activity is based on these assumptions: (i) any magma which intrudes the repository will have a low volatile content; (ii) any igneous event will involve the intrusion of a single igneous dike; (iii) the repository itself will have no effect on magma flow or eruption dynamics; (iv) magmatic events are of relatively short duration; (v) groundwater, possibly derived from a perched water table, will not interact with magma; and (vi) the probability of an intrusive event is nine times that of an extrusive event.

The current simulation model has several limitations. For example, the probability of magma activity should be related to geological faults in the repository area. The model also considers only radioactivity release for intrusive and extrusive events. The consequence analysis has not taken into account the interaction between intruding magma and a perched water table around the repository. Finally, the simulation model has not included the possibility of multiple eruptions. There is clear evidence of multiple eruptions (polycyclic activity) at most of the Quaternary cinder cones in the Yucca mountain area. The effects of this type of igneous activity remain to be included in the model.

6.4.3.4 Example of Simulation Results

The Monte Carlo simulation code VOLCANO is run on VAX 8700 at SwRI and on a CRAY Y-MP at Idaho National Engineering Laboratory (INEL). A pre-compiler program is used to ensure that

the VAX version of the FORTRAN program is compatible with the CRAY compiler. The program has three main groups of common blocks. One group of common blocks contains simulation parameters, including the dimension of the simulation system. The second group of common blocks contains variables that specify repository inventory. For example, it includes parameters about number of containers, amount of waste in a container, and other radionuclide activity information. Finally, the third group of common blocks contains parameters that specify the dimensions of arrays.

The code reads an input file VOLCANO.IN that contains simulation parameters and the repository geometry. The input simulation parameters are:

minimum area of dike
maximum area of dike
minimum length of dike
maximum length of dike
minimum width of dike
maximum width of dike
minimum dike direction angle
maximum dike direction angle
minimum cone radius
maximum cone radius

The repository geometry is divided into a total of 17 rectangular panels. The input file specifies the coordinates of the nodes that define the corners of the panel. It also contains a table that specifies the node number, the zone number, and number of waste containers for each panel. The zone number of each panel is shown in Figure 6-1.

VOLCANO code can be run in two modes. It can be run under the Total Performance Assessment (TPA) code, which determines the parameters of a magma event. In this case, VOLCANO code reads an input file that specifies the occurrence time of a magma event and parameters about the dike and cone. Alternatively, VOLCANO can be run in a standalone mode. In this mode, the occurrence time of a magma event is determined by multiplying 10,000 years by a random number between 0 and 1.

The origin of the simulation system is defined arbitrarily at the upper right corner of the 17th panel. The left boundary of the simulation system is chosen at Xmin - MaxL, where Xmin is the minimum of the x coordinates of nodes, and MaxL is the input parameter, maximum length of dike. The righthand boundary is chosen at Xmax + MaxL, where Xmax is the maximum of the x coordinates of nodes. Similarly, the lower boundary is defined at Ymin - MaxL, and the upper boundary is defined at Ymax + MaxL, where Ymin and Ymax are the minimum and maximum of the y coordinates of nodes, respectively. The dimension of the simulation system is chosen to ensure the inclusion of any magma activity that could have intercepted the repository. Figure 6-2 shows the dimensions of the simulation system for one example.

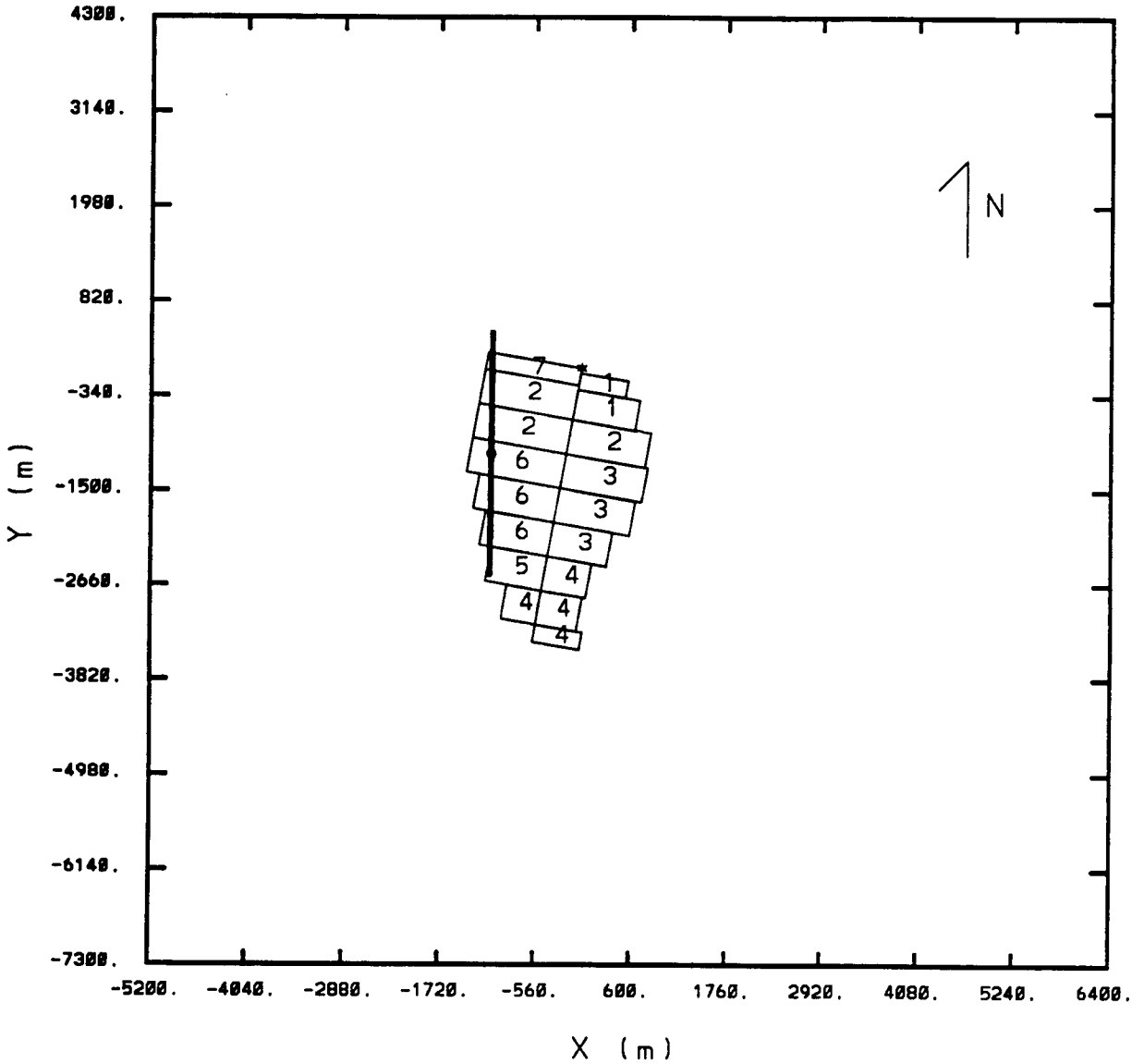

Figure 6-2. An example of a dike event from the simulation of magma scenarios. In this particular example, the dike intercepts zone 2, zone 6, and zone 7.

The output of the simulation contains:

(i) Recap of the input parameters
(ii) Recap of area and waste containers in each zone
(iii) Recap of occurrence time of the magma event and random numbers used
(iv) Coordinates of the dike and cone, length, width and angle of dike, and radius of cone.
(v) The area of the magma activity in each zone
(vi) The fraction of area intercepted by the magma activity in each zone

(vii) The number of waste containers disrupted by the magma activity
(viii) The amount of radionuclide activity released from each zone.

In addition, the simulation produces two output files VOLAIR.DAT and VOLSOT.DAT to be used as input for other modules in TPA.

Some examples of the simulation results are given in Tables 6-1 and 6-2. For illustration purposes, an igneous event is assumed to occur randomly in a time period of 10,000 years. To illustrate the consequence of volcanism, we select magma events affecting the repository. In the first example, a volcanic dike intercepts zone 2, zone 6, and zone 7 (See Table 6-1 and Figure 6-2). Table 6-1 lists Area Hit, which is the area intercepted by the magma activity in each zone. Table 6-1 shows that the amount of release is zero because dike magma events are considered to be intrusive and no radioactivity is released above the surface. Table 6-2 and Figure 6-3 illustrate the output for a cone magma event intercepting the repository. A conservative estimate of radioactivity release is made by assuming that all radioactive material intercepted by the feeder dike is released to air through the cinder cone.

6.4.3.5 Summary and Recommendation

A geometric simulation approach has been used to model the consequence of volcanism in the proposed repository. The model VOLCANO obtains the area of intersection between the repository and the area of an intrusive or extrusive magma event occurring randomly in a region surrounding the repository. The actual geometry of the proposed Yucca Mountain repository is used as input to the model. Using the repository initial inventory as input, it converts the area of interception into the number of waste containers damaged and calculates the amount of radioactivity released into the atmosphere. The predictions of the VOLCANO model, including the number of damaged waste containers and the amount of radioactivity release, are used as input by the AIRCON and SOTEC modules in the TPA code.

The main weakness of the VOLCANO model is its assumption that basaltic igneous activity occurs randomly in the region surrounding the repository with a homogeneous probability. Geological data indicate instead that the volcanic vent distribution in the Yucca Mountain area is likely clustered or related to faults. The model needs to be improved by requiring that the probability of magma activity be related to geological faults in the repository area. Furthermore, the possibility of volcanic recurrence needs to be considered. The model can be improved substantially by using the nonhomogeneous Poisson probability maps calculated by near-neighbor methods (Connor et al., 1993). Near-neighbor methods provide a more accurate assessment of volcanic recurrence at the proposed repository site than is possible through the application of homogeneous Poisson models. Finally, the consequence analysis needs to take into account the interaction between intruding magma and a perched water table around the repository. Although the model might need other improvements, these three improvements are straightforward and are recommended for immediate implementation.

Table 6-1. An example output from the simulation of magma scenarios for a dike event

Zone #	Area Hit (m^2)	Area Fraction	Number of Containers Hit (#)	Inventory per Container (Ci)
1	0.00	0.00	0	1728
2	6323	0.00445	28	1728
3	0.00	0.00	0	1728
4	0.00	0.00	0	1728
5	0.00	0.00	0	1728
6	1128	0.00088	5	1728
7	1544	0.00630	7	1728
Totals	8897	0.00161	40	

Table 6-2. An example output from the simulation of magma scenarios for a cone event

Zone #	Area Hit (m^2)	Area Fraction	Number of Containers Hit (#)	Amount of Release to Atmosphere (Ci)
1	0	0	0	0.00
2	6323	0.00445	28	48411
3	0	0	0	0.00
4	0	0	0	0.00
5	1784	0.00602	8	13831
6	11575	0.00903	51	88177
7	1544	0.00630	7	12102
Totals	21128	0.00384	94	162523

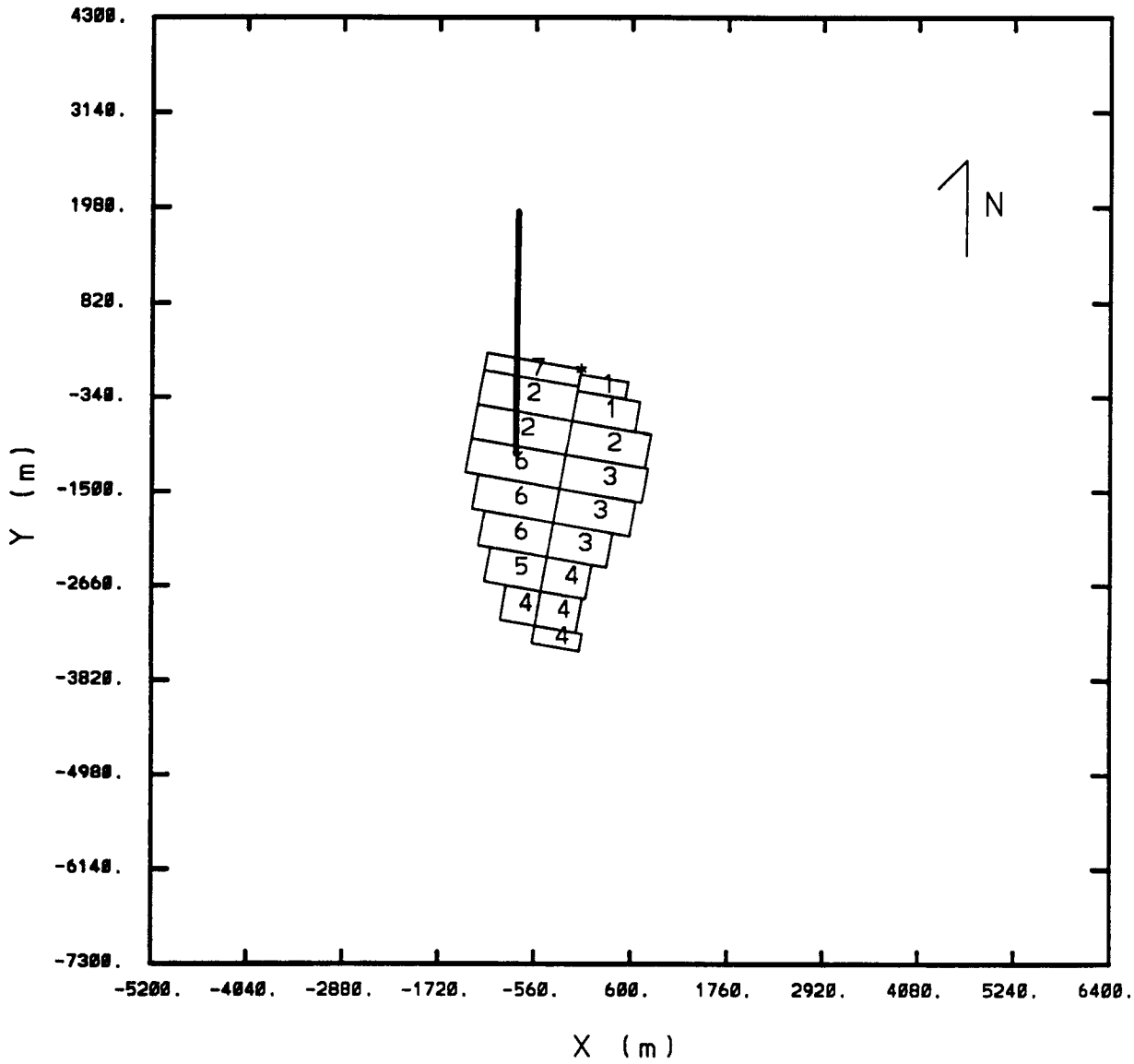

Figure 6-3. An example of a cone event from the simulation of magma scenarios. The cone represented by a circle is located in zone 6m.

6.5 REFERENCES

Connor, C.C., B.E. Hill, G.L. Stirewalt, and S.R. Young. 1993. *NRC High-Level Radioactive Waste Research at CNWRA, July 1 through December 31, 1992.* CNWRA 92-025. San Antonio, TX: Center for Nuclear Waste Regulatory Analyses.

Crowe, B.M., M.E. Johnson, and R.J. Beckman. 1982. *Calculation of the Probability of Volcanic Disruption of a High-level Radioactive Waste Repository within Southern Nevada, U.S.* Radioactive Waste Management and the Nuclear Fuel Cycle 3: 167-190.

Crowe, B.M., S. Self, D. Vaniman, R. Amos, and F. Perry. 1983. Aspects of potential magmatic disruptions of a high-level radioactive waste repository in southern Nevada. *Journal of Geology* 91:259-276.

Crowe, B.M. 1992. *Status of Probability Studies*. Panel on Structural Geology and Geoengineering Meeting on Volcanism. U.S. Nuclear Waste Technical Review Board, Sept. 14-16, 1992, Las Vegas, NV Meeting Notes.

Crowe, B.M., R. Picard, G.A. Valentine, and R.F. Perry. 1992. *Recurrence Models of Volcanic Events: Applications to Volcanic Risk Assessment*. Third Conference on Radioactive Waste Management, April 14-16, Las Vegas, NV: American Nuclear Society and American Society of Civil Engineers: 2344-2355.

Ho, C.-H. 1992. *Risk Assessment for the Yucca Mountain High-Level Nuclear Waste Repository Site: Estimation of Volcanic Disruption*. Panel on Structural Geology and Geoengineering Meeting on Volcanism. U.S. Nuclear Waste Technical Review Board, September 14-16, 1992, Las Vegas, NV Meeting Notes.

Ho, C.-H., E.I. Smith, D.L. Feurbach, and T.R. Naumann. 1991. Eruptive probability calculation for the Yucca Mountain site, USA: Statistical estimation of recurrence rates. *Bulletin of Volcanology* 54:50-56.

Margulies, T., L. Lancaster, N. Eisenberg, and L. Abramson. 1992. *Probability Analysis of Magma Scenarios for Assessing Geologic Waste Repository Performance*. American Society of Mechanical Engineers, Winter Annual Meeting, November 8-13, 1992, Anaheim, CA.

Sheridan, M.F. 1992. A Monte Carlo technique to estimate the probability of volcanic dikes. *Proceedings of the Third International Conference on High-Level Radioactive Waste Management*. Las Vegas, NV: American Nuclear Society and American Society of Civil Engineers: 2033-2038.

Smith, E.I., T.R. Feuerbach, and J.E. Faulds. 1990. The area of most recent volcanism near Yucca Mountain, Nevada: Implications for volcanic risk assessment. High-level Radioactive Waste Meeting. *Proceedings of the International Topical Meeting*. LaGrange Park, IL: American Nuclear Society 1:81-90.

Trapp, J.S. and P.S. Justus. 1992. Regulatory Requirements to Address Issues Related to Volcanism and Magmatism: Code of Federal Regulations, Title 10, Part 60, Disposal of High-Level Radioactive Wastes in Geological Repositories. *Proceedings of the Third International Conference on High Level Radioactive Waste Management*: 2039-2046.

Valentine, G.A., B.M. Crowe, and F.V. Perry. 1992. Physical Processes and Effects of Magmatism in the Yucca Mountain Region. *Proceedings of the Third International Conference on High-Level Radioactive Waste Management*. Las Vegas, NV: American Nuclear Society and American Society of Civil Engineers: 2014-2024.